J. Fluid Mech. (2010), *vol.* 645, *pp.* 145–185.
doi:10.1017/S0022112009992539

Shear-layers in magnetohydrodynamic spherical Couette flow with conducting walls

A. M. SOWARD[1]† AND E. DORMY[2]

[1]Mathematics Research Institute, School of Engineering, Computer Science & Mathematics, University of Exeter, Harrison Building, North Park Road, Exeter EX4 4QF, UK

[2]MHD in Astro- & Geophysics (ENS/IPGP) & CNRS, LRA, Département de Physique, Ecole Normale Supérieure, 24, rue Lhomond, 75231 Paris Cedex 05, France

(Received 16 January 2009; revised 27 September 2009; accepted 30 September 2009; first published online 2 February 2010)

We consider the steady axisymmetric motion of an electrically conducting fluid contained within a spherical shell and permeated by a centred axial dipole magnetic field, which is strong as measured by the Hartmann number M. Slow axisymmetric motion is driven by rotating the inner boundary relative to the stationary outer boundary. For $M \gg 1$, viscous effects are only important in Hartmann boundary layers adjacent to the inner and outer boundaries and a free shear-layer on the magnetic field line that is tangent to the outer boundary on the equatorial plane of symmetry. We measure the ability to leak electric current into the solid boundaries by the size of their relative conductance ε. Since the Hartmann layers are sustained by the electric current flow along them, the current inflow from the fluid mainstream needed to feed them increases in concert with the relative conductance, because of the increasing fraction $\mathscr{L}$ of the current inflow leaked directly into the solids. Therefore the nature of the flow is sensitive to the relative sizes of ε^{-1} and M.

The current work extends an earlier study of the case of a conducting inner boundary and an insulating outer boundary with conductance $\varepsilon_o = 0$ (Dormy, Jault & Soward, *J. Fluid Mech.*, vol. 452, 2002, pp. 263–291) to other values of the outer boundary conductance. Firstly, analytic results are presented for the case of perfectly conducting inner and outer boundaries, which predict super-rotation rates Ω_{max} of order $M^{1/2}$ in the free shear-layer. Successful comparisons are made with numerical results for both perfectly and finitely conducting boundaries. Secondly, in the case of a finitely conducting outer boundary our analytic results show that Ω_{max} is $O(M^{1/2})$ for $\varepsilon_o^{-1} \ll 1 \ll M^{3/4}$, $O(\varepsilon_o^{2/3} M^{1/2})$ for $1 \ll \varepsilon_o^{-1} \ll M^{3/4}$ and $O(1)$ for $1 \ll M^{3/4} \ll \varepsilon_o^{-1}$. On increasing ε_o^{-1} from zero, substantial electric current leakage into the outer boundary, $\mathscr{L}_o \approx 1$, occurs for $\varepsilon_o^{-1} \ll M^{3/4}$ with the shear-layer possessing the character appropriate to a perfectly conducting outer boundary. When $\varepsilon_o^{-1} = O(M^{3/4})$ the current leakage is blocked near the equator, and the nature of the shear-layer changes. So, when $M^{3/4} \ll \varepsilon_o^{-1}$, the shear-layer has the character appropriate to an insulating outer boundary. More precisely, over the range $M^{3/4} \ll \varepsilon_o^{-1} \ll M$ the blockage spreads outwards, reaching the pole when $\varepsilon_o^{-1} = O(M)$. For $M \ll \varepsilon_o^{-1}$ current flow into the outer boundary is completely blocked, $\mathscr{L}_o \ll 1$.

† Email address for correspondence: a.m.soward@exeter.ac.uk

1. Introduction

The steady flow of viscous fluid confined inside a spherical shell, which results when the inner (radius r_i^*) and outer (radius r_o^*) solid boundaries rotate at different angular velocities, namely Ω_i^{S*} and Ω_o^{S*} respectively, about a common axis, is referred to as spherical Couette flow. In recent years its magnetohydrodynamic (MHD) extension, for which the fluid is electrically conducting and is permeated by a magnetic field applied externally, has attracted considerable attention. One reason for the interest is geophysical. In particular, the electromagnetic coupling between the conducting fluid outer core and the poorly conducting solid mantle may play an important role in Earth's dynamo process and may in addition affect relatively short-time scale phenomenon such the variation in Earth's length of day (see, e.g., Zatmann 2001). Another reason is astrophysical and concerns the rotation rate of the solar radiative zone (see, e.g., Garaud & Guervilly 2009). Further interest stems from laboratory models that involve MHD spherical Couette flow (see, e.g., Nataf *et al.* 2006; Kelley *et al.* 2007), which are motivated by the geophysical application.

Like others before, we will consider a steady axial dipole magnetic field of typical strength B_0^* maintained by electromagnetic sources within the inner sphere. We will assume that the outer sphere is stationary, $\Omega_o^{S*} = 0$. Using the fluid shell gap width $L^* \equiv r_o^* - r_i^*$ as our unit of length, the magnetic field strength and the importance of advection are measured by the Hartmann and magnetic Reynolds numbers,

$$M \equiv \frac{L^* B_0^*}{\sqrt{\mu_0 \rho \nu \eta}} \qquad \text{and} \qquad Re_M \equiv \frac{L^{*2} \Omega_i^{S*}}{\eta} \tag{1.1a,b}$$

respectively, where ρ is the density; ν is the viscosity; μ_0 is the magnetic permeability; and η is the magnetic diffusivity. We restrict attention to strong magnetic fields and slow steady flow which correspond to the limits

$$M \gg 1 \qquad \text{and} \qquad Re_M \ll 1 \tag{1.2a,b}$$

respectively. The latter assumption, $Re_M \ll 1$, ensures that the magnetic field perturbations are small and is essentially the basis on which we linearize our equations. We add the assumption that the Reynolds number $Re \equiv L^{*2} \Omega_i^{S*} / \nu$ is sufficiently small (really a condition on the magnetic Prandtl number $\eta/\nu \equiv Re/Re_M$) in order that we may restrict attention to the axisymmetric differential rotation of the fluid and ignore any meridional secondary flow, including possible instabilities, in our equation of motion (2.7*a*).

In the large-M limit (1.2*a*), viscous forces are negligible in the bulk of the flow, called the mainstream, but are important in various boundary and free shear-layers. Hartmann layers of width $\delta_H^* \equiv \sqrt{\mu_0 \rho \nu \eta}/B_0^* = L^*/M$ form on the inner and outer boundaries. Their properties, which have been studied extensively since the pioneering theoretical and experimental investigations of Hartmann (1937) and Hartmann & Lazarus (1937) (see also the review of Hunt & Shercliff 1971), are crucial to our development. Since the Hartmann layer width is inversely proportional to the magnitude of the normal component of magnetic field, its width is very large on the outer boundary close to the 'equatorial' plane (i.e. plane of symmetry), where the dipole magnetic field lines are tangent to the boundary. We give the label $\mathscr{C}$ to the magnetic field line that touches the outer boundary at the point E_o on the equator (see figure 1). The outer Hartmann layer becomes singular at E_o, forming a Roberts layer (Roberts 1967*b*), which in turn triggers a free shear-layer on the magnetic field line $\mathscr{C}$ of width $\delta_{\mathscr{C}}^* \equiv \sqrt{L^* \delta_H^*} = L^*/M^{1/2}$, which continues until $\mathscr{C}$ intersects the inner

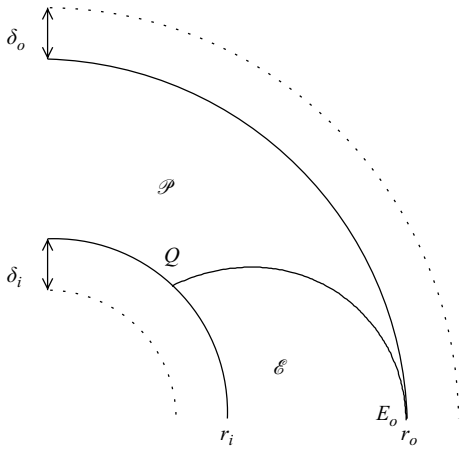

FIGURE 1. The northern hemisphere geometry (here for an aspect ratio of $\zeta_i \equiv r_i/r_o = 1/2$). At large M, the polar $\mathscr{P}$ and equatorial $\mathscr{E}$ mainstream regions are separated by the shear-layer containing the magnetic field line $\mathscr{C}$ joining E_o to Q. The widths of the inner and outer solid shell boundaries are δ_i and δ_o respectively.

sphere at a point Q. Free shear-layers of this thickness have been found in other MHD contexts (see Hunt & Malcolm 1968; see also Müller & Bühler 2001), though similar sidewall layers are perhaps more common (see, e.g., Roberts 1967*a*). Other related free layers, such as those of Stewartson (1966), pertain to rapidly rotating flows and have been surveyed by Soward & Dormy (2007). The presence of the shear-layers on $\mathscr{C}$-lines in the shell was clearly identified by the numerical simulations of Dormy, Cardin & Jault (1998; see also Dormy 1997 and the discussion of Starchenko 1998*a*,*b*). Surprisingly Dormy *et al.* (1998) found, for the case of a conducting inner and insulating outer boundary, that the angular velocity in these $M^{-1/2}$ shear-layers exceeded by about 50 % the angular velocity Ω_i^{S*} of the inner sphere. This so called super-rotation was later confirmed by the liquid sodium experiments of Nataf *et al.* (2006).

The subsequent theoretical investigations of Hollerbach (2000, 2001) and Hollerbach & Skinner (2001) drew attention to the fact that the magnitude of the super-rotation is strongly dependent on the electrical conductivities of the solid boundaries, which have a controlling influence on the electric current flow throughout the entire system, both fluid and solid. To understand this phenomenon, we begin by noting that viscous forces are negligible in the mainstream. There the Lorentz force, which dominates the dynamics, is un-balanced and negligible. As is well known, this force-free configuration is achieved by the electric current being channelled along the lines of the applied magnetic field. On leaving the mainstream, this electric current flows partly along the Hartmann layers and partly through their adjacent solid boundaries in proportions dependant on the relative conductance of the of the solids to the fluid. Any net current inflow or outflow across the mainstream must finally be returned along the free shear-layer which embeds the $\mathscr{C}$-line.

In the case of an inner conducting boundary and an outer insulating boundary, first considered by Dormy *et al.* (1998), electric current flow in the outer insulating boundary is blocked off entirely. So only a relatively small amount of electric current from the mainstream is needed to feed the outer boundary Hartman layer. To achieve this small-electric-current flow in the mainstream, it is necessary that the azimuthal

magnetic field produced by magnetic induction must be small too. In a steady state, this requirement constrains the angular velocity Ω^* to be almost constant on field lines, which is the 'law of isorotation' of Ferraro (1937). Effectively, the magnetic field is almost frozen to the fluid. Thus, the fluid in the mainstream locks on to the inner conducting boundary and rotates solidly with angular velocity $\Omega^* = \Omega_i^{S*}$; the entire angular velocity jump Ω_i^{S*} is accommodated across the outer boundary Hartmann layer. The electric current in this Hartmann layer flows towards the equator, from where it is returned to the inner solid sphere along the narrow shear-layer embedding the $\mathscr{C}$-line. The resulting relatively large electric current density in the shear-layer leads to a large Lorentz force, which drives the super-rotation. Dormy *et al.* (2002) provided a detailed numerical and analytic investigation of this case.

On letting the outer boundary have even a small electrical conductivity, currents leak into the solid, and to maintain the same current flow in the Hartmann layers, the electric current flow in the mainstream must increase. In short, the induced azimuthal magnetic field must increase in concert with the outer boundary conductivity. So, when the conductivity of both the inner and outer boundaries is comparable to that of the fluid, the electric current in the mainstream is so large that to maintain it by magnetic induction, Ω^* is no longer constant on field lines and Ferraro's law of isorotation is violated. Indeed these ideas are consistent with the numerical results of Hollerbach (2000, 2001) and Hollerbach & Skinner (2001), who also found that the super-rotation increases in concert with the outer boundary conductivity.

One of the main obstacles to obtaining analytic solutions for the case of boundaries with finite electrical conductivity is that a potential problem for the magnetic field must be solved in the solids. Consequently the required magnetic field boundary conditions at the solid–fluid interface are non-local and depend on the solution of the potential problems in the solids, except in the perfectly conducting or insulating limits. The difficulty may be avoided by considering thin shell boundaries, for which a local boundary condition can be constructed (see, e.g. Shercliff 1956; Walker 1981). Indeed, such an assumption may well be very reasonable for laboratory dynamos. The works of Hollerbach, Canet & Fournier (2007) and Mizerski & Bajer (2007) have taken advantage of this approximation and have considered a thin outer boundary of relative conductance ε_o (see (2.31*c*)), which provides a measure of the capability of the boundary to carry electric current; $\varepsilon_o = 0$ for an insulating boundary and $\varepsilon_o^{-1} = 0$ for a perfectly conducting boundary.

Mizerski & Bajer (2007) extended the asymptotic analysis for $M \gg 1$ of Dormy *et al.* (2002) to include the case of a finitely conducting outer boundary. Though most of their analysis is restricted to a plane layer geometry, the mechanisms, which they found, can be identified in spherical geometry. The main limitation of their analysis is that they restricted attention to the case of only a very small relative conductance $\varepsilon_o = O(M^{-1})$. In this range they reported only a small increase $O(\varepsilon_o M^{3/4} \Omega_i^{S*})$ of the super-rotation rate. Indeed, on increasing ε_o, Mizerski & Bajer (2007) left the parameter regime for which their asymptotic analysis is valid. They did, however, obtain numerical solutions of the complete system of governing partial differential equations for $\varepsilon_o = O(1)$. Even so, Mizerski & Bajer (2007) were unable to find super-rotation rates of magnitude $O(M^{1/2} \Omega_i^{S*})$, predicted by the numerical results of Hollerbach *et al.* (2007) for spherical shell (as opposed to plane layer) geometry.

Bühler (2009) considered the case of concentric cylindrical shell boundaries together with an applied uniform axial magnetic field. For his choice of perfectly conducting inner and outer boundaries, Bühler (2009) identified the importance of the electric potential ϑ^*, which defines the electric field $\boldsymbol{E}^* = -\nabla^* \vartheta^*$. Since the 'relative' electric

potential on each boundary, i.e. as measured in the frame co-rotating with that boundary, is constant and since the 'true' electric potential is continuous across the Hartmann layers, the mainstream value of $\vartheta^* = O(L^{*2}\Omega_i^{S*}B_0^*)$ is readily determined and is found to exhibit a jump $\Theta_{\mathscr{C}}^*$ of the same size across the $\mathscr{C}$-line. In consequence, the azimuthal angular velocity $\Omega_{\mathscr{C}}^*$ inside the free shear-layer is necessarily large, inducing a jump of the electric potential across it of magnitude $\delta_{\mathscr{C}}^* L^* \Omega_{\mathscr{C}}^* B_0^*$. This equals $\Theta_{\mathscr{C}}^*$ when $\delta_{\mathscr{C}}^* \Omega_{\mathscr{C}}^* \sim L^* \Omega_i^{S*}$ with the physical interpretation that the azimuthal volume flux carried inside the shear-layer is the same order of magnitude as that carried by the main bulk of the flow in the mainstream. Furthermore, since $\delta_{\mathscr{C}}^* = L^*/M^{1/2}$, we conclude that the magnitude of the shear-layer super-rotation is $\Omega_{\mathscr{C}}^* = O(M^{1/2}\Omega_i^{S*})$. In contrast, when the inner and outer boundaries are perfectly conducting and insulating respectively, the jump in the electric potential across the layer is almost totally eliminated and then $\Omega_{\mathscr{C}}^* = O(\Omega_i^{S*})$. Nevertheless, as found by Dormy *et al.* (2002), the super-rotation still exists because the maximum value of $\Omega_{\mathscr{C}}^*$ exceeds Ω_i^{S*}.

The outline of our paper is as follows. In § 2 we formulate the mathematical problem and describe the spatial domain structure appropriate to the large-Hartmann-number limit. The mainstream problem outside the Hartmann boundary layers and free shear-layer on the $\mathscr{C}$-line is developed in § 2.1; the Hartmann boundary layer jump conditions are derived in § 2.2; the mainstream problem is completed on making the thin solid boundary approximation in § 2.3. It should be remarked that this approximation is not necessary in the limiting cases of perfectly conducting or insulating boundaries.

The case of perfectly conducting boundaries is investigated in detail in § 3 by both analytic and numerical methods, like Bühler (2009) before. Unlike Bühler (2009), our applied magnetic field lines are not generally normal to the boundaries. So their oblique intersection causes our mainstream electric current channelled by the field lines to possess a component parallel to the boundaries. According to Ohm's law that, in turn, leads to a tangential component of the 'relative' electric field (as measured in the reference frame rotating with the fluid), which is the *raison d'être* for our Hartmann layers. In the model of Bühler (2009), Hartmann layers are absent because of the orthogonal intersection of the uniform applied magnetic field with the boundaries. In § 3.1 and Appendix A, we present the analytic solution of our mainstream problem and compare the results with those of the complete governing partial differential equations; they are contrasted with the results for thick boundaries possessing the same electrical conductivity as the fluid in § 3.2 in order to test the limitations of the perfect-conductivity approximation. We formulate the shear-layer problem in § 3.3 and Appendix B; numerical solutions of the shear-layer equations are provided in § 3.4.

In § 4 we consider the case of a perfectly conducting inner boundary together with a thin outer boundary of relative conductance ε_o. We investigate the limit $M \uparrow \infty$ in § 4.1; numerical solutions of the mainstream problem are found for the $\varepsilon_o = O(1)$ case, while for the $\varepsilon_o \ll 1$ case analytic solutions are given in Appendix C. We consider the nature of the double limit $M \gg 1$, $\varepsilon_o \ll 1$ in § 4.2, where we discuss the role of the outer Hartmann layer, whose width is measured conveniently by the inverse of a latitudinally dependent local Hartmann number M_o^{loc}, introduced in § 2.2, based on the magnitude of the radial component of the applied dipole magnetic field on the outer boundary. It decreases in size from $O(M)$ at the pole to $M_{o\mathscr{C}}^{loc} = O(M^{3/4})$ near the equator on the shear-layer length scale. The fraction $\mathscr{L}_o$ of the mainstream electric current entering the Hartmann layer but then leaked directly into the solid boundary is dependent on the product $\varepsilon_o M_o^{loc}$. The nature of the shear-layer, however, is determined by the leakage $\mathscr{L}_{o\mathscr{C}}$ at the equator, which depends on $\varepsilon_o M_{o\mathscr{C}}^{loc}$. It is this

physical feature which flags the importance of the product $\varepsilon_o M^{3/4}$ previously identified in the analysis of Mizerski & Bajer (2007). The form taken by the shear-layer problem, when $\varepsilon_o M^{3/4} = O(1)$, is outlined in § 4.3, while the implied estimates for the magnitude of the super-rotation are given in § 5.1. Having absorbed the mathematical formulation of the problem in § 2, the reader might benefit from skimming the contents of our concluding § 6, where we elaborate on these parameter range considerations, before studying the intervening sections.

The results of §§ 4 and 5.1 are extended to the case of an inner solid thin shell boundary of finite conductance $\varepsilon_i = 1$ in § 5.2 so that we can make some tentative, yet encouraging, comparisons with the numerical results obtained by Hollerbach *et al.* (2007).

2. Formulation

We adopt $L^*(\equiv r_o^* - r_i^*)$, $L^*\Omega_i^{S*}$, B_0^*, $L^*\Omega_i^{S*}B_0^*$ and $B_0^*/(\mu_0 L^*)$ as our units of length, velocity, magnetic field, electric field and electric current respectively. The superscript '*' is dropped for all dimensionless quantities so that, for example, the fluid shell gap width and inner boundary angular velocity are $r_o - r_i = 1$ and $\Omega_i^S = 1$ respectively (see (2.10)).

Relative to cylindrical polar coordinates (s, ϕ, z), we denote points (s, z) on the inner and outer boundaries by (s_i, z_i) and (s_o, z_o) respectively. Our applied dipole magnetic field $\boldsymbol{B}_M$ is represented by

$$\boldsymbol{B}_M = s^{-1}\nabla A \times \widehat{\boldsymbol{\phi}} = -\nabla\Phi, \tag{2.1a}$$

where $\widehat{\boldsymbol{\phi}}$ is the unit vector in the azimuthal direction, which has the properties

$$\boldsymbol{B}_M \cdot \nabla A = 0 \qquad \text{and} \qquad -\boldsymbol{B}_M \cdot \nabla\Phi = |\boldsymbol{B}_M|^2 = s^{-2}|\nabla A|^2. \tag{2.1b,c}$$

Here $\boldsymbol{B}_M$ is normalized by the choice

$$A \equiv \tfrac{1}{2}s^2 r^{-3}, \qquad \Phi \equiv \tfrac{1}{2}zr^{-3} \qquad (r \equiv \sqrt{s^2+z^2}). \tag{2.2a,b}$$

Relative to spherical polar coordinates (r, θ, ϕ), the radial and azimuthal (r, θ) components of magnetic field determine the useful relations

$$rB_r = \frac{1}{s}\frac{\partial A}{\partial\theta} = -r\frac{\partial\Phi}{\partial r} = 2\Phi, \tag{2.3a}$$

$$rB_\theta = -\frac{\partial\Phi}{\partial\theta} = -\frac{r}{s}\frac{\partial A}{\partial r} = \frac{A}{s}. \tag{2.3b}$$

Furthermore, (2.2*a*,*b*) may be used to express s and Φ as functions of A and r,

$$s/r = \sqrt{2rA}, \qquad 2r^2\Phi = (\operatorname{sgn} z)\sqrt{1-2rA}, \tag{2.4a,b}$$

which are used to determine the boundary values (2.13*a*,*b*). In terms of (r, A) coordinates, the area element $\mathrm{d}\mathscr{S} \equiv \mathrm{d}s\,\mathrm{d}z$ weighted by s may be expressed as

$$s\,\mathrm{d}\mathscr{S} = \frac{r}{2\Phi}\,\mathrm{d}r\,\mathrm{d}A. \tag{2.4c}$$

Points on the magnetic field line $\mathscr{C} : A = A_c \equiv 1/2r_o$, which touches the outer sphere boundary tangentially at the equator $E_o : (r_o, 0)$, are denoted by (s_c, z_c). This $\mathscr{C}$-line intersects the inner sphere boundary at $Q : (s_Q, z_Q)$ (see figure 1) and divides the northern hemisphere, $z \geqslant 0$, of the fluid shell up into two regions $\mathscr{P} : A < A_c$

and $\mathscr{E}$: $A > A_c$. In the former polar region $\mathscr{P}$ the magnetic field lines intersect both the inner and outer shell boundaries, $r = r_i$ and $r = r_o$. In the latter equatorial region $\mathscr{E}$ the magnetic field lines intersecting the inner sphere boundary cross the equator within the fluid and return to the inner sphere without ever meeting the outer spherical boundary. For our analysis of the free shear-layer on $\mathscr{C}$, we will find it convenient to employ the equatorial Hartmann number

$$\mathscr{M} \equiv \frac{M}{2r_o^2} \tag{2.5}$$

introduced by Dormy *et al.* (2002), which is based on the local magnetic field strength $B_0^*/2r_o^3$ at E_o and the length r_o^*.

For our choice of units, the slow steady azimuthal velocity $\boldsymbol{u} = (0,\ s\Omega,\ 0)$ forced by rotating the inner sphere induces small magnetic field perturbations $(0,\ Re_M B,\ 0)$. By Ampère's law the corresponding electric current $Re_M \boldsymbol{j}$ is determined by

$$\boldsymbol{j} = s^{-1}\nabla(sB) \times \widehat{\boldsymbol{\phi}}. \tag{2.6a}$$

Just as A is a 'stream function' for the applied magnetic field $\boldsymbol{B}_M$ providing a measure of magnetic flux, so is sB a 'stream function' for $\boldsymbol{j}$ measuring electric current flux. The electric field perturbation $\boldsymbol{E}$ is related to $\boldsymbol{j}$ by Ohm's law $\boldsymbol{j} = \sigma(\boldsymbol{E} + \boldsymbol{u} \times \boldsymbol{B}_M)$, where σ is a dimensionless measure of the electrical conductivity taking the value unity in the fluid. For our steady state, we have $\nabla \times \boldsymbol{E} = 0$, and so we may write $\boldsymbol{E} = -\nabla\vartheta$, where ϑ is the electric potential. Then Ohm's law determines

$$\boldsymbol{j} = -\sigma\,(\nabla\vartheta\ -\ \Omega\,\nabla A). \tag{2.6b}$$

From (2.6*a*,*b*) the θ-components of electric current j_θ and field $E_\theta = -r^{-1}\partial\vartheta/\partial\theta$ are related by

$$j_\theta = -\frac{1}{s}\frac{\partial(sB)}{\partial r} = -\frac{\sigma}{r}\left(\frac{\partial\vartheta}{\partial\theta}\ -\ \Omega\,\frac{\partial A}{\partial\theta}\right). \tag{2.6c}$$

Our choice of units is guided by the properties of the fluid in the region $r_i < r < r_o$, where by construction $\sigma = 1$ in (2.6*b*,*c*). On linearizing the equations of motion and magnetic induction on the basis that Re and Re_M are small, their ϕ-components give

$$M^2 s^{-1}\,\boldsymbol{B}_M \cdot \nabla\,(sB)\ +\ (\nabla^2\ -\ s^{-2})(s\Omega) = 0, \tag{2.7a}$$

$$s\,\boldsymbol{B}_M \cdot \nabla\,\Omega\ +\ (\nabla^2\ -\ s^{-2})B = 0 \tag{2.7b}$$

respectively. In view of (2.6*b*) the Lorentz force $M^2(s^{-1}\boldsymbol{B}_M \cdot \nabla(sB))\widehat{\boldsymbol{\phi}}$ appearing in (2.7*a*) has the alternative representation

$$M^2\,\boldsymbol{j} \times \boldsymbol{B}_M\ =\ M^2(s^{-1}(\nabla\vartheta) \cdot (\nabla A)\ -\ |\boldsymbol{B}_M|^2\,s\Omega)\,\widehat{\boldsymbol{\phi}}. \tag{2.8}$$

We take advantage of the symmetry $A(s, -z) = A(s, z)$ of the applied dipole field and assume that in consequence, $\Omega(s, -z) = \Omega(s, z)$, $\vartheta(s, -z) = \vartheta(s, z)$ and $B(s, -z) = -B(s, z)$. Respectively, they imply

$$\frac{\partial\Omega}{\partial z} = \frac{\partial\vartheta}{\partial z} = B = 0 \qquad \text{on the equator} \quad z = 0. \tag{2.9}$$

In order to avoid unnecessary sign complications, we henceforth restrict attention to the upper half-sphere $z \geqslant 0$.

The fluid is bounded inside and outside by rigid boundaries on which the angular velocities are

$$\Omega = \Omega^S_{(i,o)} \equiv \begin{cases} 1 & \text{on} \quad r = r_i, \\ 0 & \text{on} \quad r = r_o. \end{cases} \tag{2.10}$$

The inner and outer rigid boundaries are electrically conducting shells of thickness δ_i and δ_o, and their respective dimensionless conductivities $\sigma = \sigma^S_i$ and $\sigma = \sigma^S_o$ generally differ from the value $\sigma = 1$ of the fluid. More precisely, $\sigma^S_{(i,o)}$ is the conductivity ratio of the solid to fluid. Inside these solids Ohm's law (2.6*b*) reduces to $\boldsymbol{j} = -\sigma^S_{(i,o)}\nabla(\vartheta - \Omega^S_{(i,o)}A)$ with the consequence that $\nabla \times \boldsymbol{j} = 0$, and by implication the magnetic field satisfies

$$(\nabla^2 - s^{-2})B = 0 \qquad \text{in} \quad \begin{cases} r_i - \delta_i < r < r_i, \\ r_o < r < r_o + \delta_o. \end{cases} \tag{2.11}$$

Across each of the fluid–solid interfaces the tangential magnetic and electric fields are continuous:

$$B, \qquad E_\theta \quad \text{and} \quad \sigma^{-1} j_\theta \qquad \text{are continuous across} \quad r = r_{(i,o)}. \tag{2.12a}$$

The continuity of $\sigma^{-1} j_\theta$ follows from Ohm's law because the no-slip condition ensures that $\boldsymbol{u} \times \boldsymbol{B}_M$ is continuous The regions $r < r_i - \delta_i$ and $r_o + \delta_o < r$ beyond the shells (when they exist, i.e. $\delta_i < r_i$ and $\delta_o < \infty$) are vacuums, where $B = 0$. On application of the boundary condition, B continuous across the solid–vacuum interface, we obtain the condition

$$B = 0 \quad \text{on} \quad r = r_{(i,o)} - \varsigma_{(i,o)}\delta_{(i,o)}, \qquad \text{where} \quad \begin{cases} \varsigma_i = 1, \\ \varsigma_o = -1. \end{cases} \tag{2.12b}$$

In our development below, we will use the subscripts i and o to denote values on $r = r_i$ and $r = r_o$ on the same magnetic field line $A =$ constant. Accordingly all functions labelled by the subscripts i and o are functions of A alone. So, for example, (2.4*a*,*b*) determine

$$s_{(i,o)}(A) = r_{(i,o)}\sqrt{2r_{(i,o)}A}, \qquad \Phi_{(i,o)}(A) = \tfrac{1}{2} r^{-2}_{(i,o)}\sqrt{1 - 2r_{(i,o)}A}, \tag{2.13a,b}$$

where the positive value of the square root in (2.4*b*) has been taken as we restrict attention to the region $z \geqslant 0$. For any scalar function such as the electric potential ϑ evaluated at the inner or outer boundary, the θ-derivative of $\vartheta_{(i,o)}(A)$, using (2.3*a*), satisfies

$$\left(\frac{1}{s}\frac{\partial \vartheta}{\partial \theta}\right)_{(i,o)} = \frac{1}{s_{(i,o)}}\frac{\partial \vartheta_{(i,o)}}{\partial \theta} = \left(\frac{1}{s}\frac{\partial A}{\partial \theta}\right)_{(i,o)} \vartheta'_{(i,o)} = 2\Phi_{(i,o)}\,\vartheta'_{(i,o)}, \tag{2.14a}$$

where, here and henceforth, the prime denotes differentiation with respect to A. On replacing ϑ by Φ in (2.14*a*) and using (2.2*a*) and (2.3*b*), we obtain

$$(4r^3\Phi)_{(i,o)}\,\Phi'_{(i,o)} = \left(\frac{2r^3}{s}\frac{\partial \Phi}{\partial \theta}\right)_{(i,o)} = -1, \tag{2.14b}$$

which, together with

$$B_{r(i,o)} = (2r^{-1}\Phi)_{(i,o)} \tag{2.14c}$$

(see (2.3*a*)), is central to our large-Hartmann-number asymptotics.

To help clarify the subsequent development, we summarize our labelling conventions. We identify the values of functions on the inner i or outer o boundaries,

the $\mathscr{C}$-line and at the point Q by the subscripts i, o, c and Q respectively, e.g.

$$\Phi_{(i,o)}(A) \equiv \Phi(r_{(i,o)},\ A), \qquad \Phi_c(r) \equiv \Phi(r,\ A_c), \qquad \Phi_Q \equiv \Phi(r_i,\ A_c). \quad (2.15a,b,c)$$

The notation $(\ldots)_{(i,o)}$ means that everything inside the brackets is evaluated at either the i or the o boundary, e.g. in (2.14c), $(2r^{-1}\Phi)_{(i,o)} \equiv 2r^{-1}_{(i,o)}\Phi_{(i,o)}$. The values of mainstream functions at the locations identified by (2.15) may differ from the actual values inside the adjacent boundary or shear-layer. So, for example, the mainstream values $\Omega_{(i,o)}$ of the angular velocity Ω generally differ from the boundary values $\Omega^S_{(i,o)}$, where the superscript S is used to denote values in the solids.

2.1. *The mainstream solution*

In the large-Hartmann-number limit

$$M \gg 1 \tag{2.16}$$

for which our asymptotic analysis is valid, viscous dissipation in the mainstream exterior to all boundary layers is negligible at leading order. With the neglect of viscosity and the absence of an azimuthal pressure gradient, the azimuthally directed Lorentz force is unopposed and thus vanishes. The consequence of $\boldsymbol{j} \times \boldsymbol{B}_M \approx 0$ is that the electric current lines, $sB =$ constant, are aligned with the meridional magnetic field lines, $A =$ constant, consistent with the implication $\boldsymbol{B}_M \cdot \nabla(sB) = O(M^{-2})$ of (2.7a). We therefore introduce the electric current flux function $-\mathscr{G}(A)$ defined by

$$sB = -\mathscr{G} + O(M^{-2}), \tag{2.17a}$$

from which we deduce that the electric current (2.6a) is

$$\boldsymbol{j} = \mathscr{J}\,\boldsymbol{B}_M + O(M^{-2}), \qquad \mathscr{J} \equiv -\mathscr{G}' \tag{2.17b}$$

and hence from (2.3b) that

$$rsj_\theta = A\,\mathscr{J} + O(M^{-2}). \tag{2.17c}$$

Then from Ohm's law (2.6b) with $\sigma = 1$, we obtain

$$\nabla\vartheta = \Omega\,\nabla A + \mathscr{J}\,\nabla\Phi + O(M^{-2}) \tag{2.18a}$$

or, equivalently,

$$\nabla(\vartheta - \Phi\mathscr{J}) = (\Omega - \Phi\,\mathscr{J}')\,\nabla A + O(M^{-2}). \tag{2.18b}$$

Integration of (2.18b) shows that

$$\vartheta - \Phi\,\mathscr{J} = \mathscr{T}(A) + O(M^{-2}), \tag{2.19a}$$

where

$$\Omega - \Phi\,\mathscr{J}' = \mathscr{F}(A) + O(M^{-2}), \qquad \mathscr{F} \equiv \mathscr{T}'. \tag{2.19b}$$

Here Φ and, in consequence, both ϑ and Ω should be interpreted as functions of A and r (see (2.4b)).

When the perturbation magnetic field B in the mainstream is small, the Ohmic diffusion term $(\nabla^2 - s^{-2})B$ in the magnetic induction equation (2.7b) is negligible. This leaves $\boldsymbol{B}_M \cdot \nabla\Omega = 0$, implying that the angular velocity $\Omega =$ constant on field lines (i.e. small $\mathscr{J}'$ and $\Omega \approx \mathscr{F}(A)$). This is the law of isorotation of Ferraro (1937), which possesses the corollary that the electric potential is also constant on field lines (i.e. small $\mathscr{J}$ and $\vartheta \approx \mathscr{T}(A)$). More generally, we find (see § 3.1) that the neglect of Ohmic dissipation is unjustified and that the Ohmic diffusion term needs to be

retained in our leading-order approximation of (2.7*b*). Then Ferraro's law $\Omega \approx \mathscr{F}(A)$ and its corollary $\vartheta \approx \mathscr{T}(A)$ are broken by the additional contributions $\Phi\mathscr{J}$ and $\Phi\mathscr{J}'$ in (2.19*a*,*b*) to ϑ and Ω respectively, which are no longer functions of A alone.

In the equatorial region $\mathscr{E} : A_c \equiv 1/2r_o < A \leqslant 1/2r_i$, we note that the boundary condition $B = 0$ on $z = 0$ (see (2.9)) implies that

$$\mathscr{G} = 0. \tag{2.20a}$$

Substitution of $\mathscr{J} = -\mathscr{G}' = 0$ into (2.19*a*,*b*) determines

$$\vartheta = \mathscr{T} + O(M^{-2}), \qquad \Omega = \mathscr{T}' + O(M^{-2}), \tag{2.20b,c}$$

where $\mathscr{T}(A)$ is ultimately determined by the Hartmann jump condition at the inner shell boundary $r = r_i$.

In the polar region $\mathscr{P} : 0 \leqslant A < A_c$, we denote the mainstream values of ϑ, Ω next to the inner and outer boundaries by $\vartheta_{(i,o)}(A)$, $\Omega_{(i,o)}(A)$ and rewrite (2.19*a*,*b*) in the form

$$\vartheta = \vartheta_{(i,o)} + (\Phi - \Phi_{(i,o)})\,\mathscr{J} + O(M^{-2}), \tag{2.21a}$$

$$\Omega = \Omega_{(i,o)} + (\Phi - \Phi_{(i,o)})\,\mathscr{J}' + O(M^{-2}), \tag{2.21b}$$

where $\Phi_{(i,o)}(A)$ are defined by (2.13*b*). Since (2.21*a*,*b*) are pairs of equations, elimination of ϑ and Ω in each pair determines the electric potential and angular velocity jumps

$$\vartheta_i - \vartheta_o = (\Phi_i - \Phi_o)\,\mathscr{J} + O(M^{-2}), \tag{2.21c}$$

$$\Omega_i - \Omega_o = (\Phi_i - \Phi_o)\,\mathscr{J}' + O(M^{-2}) \tag{2.21d}$$

across the mainstream between the inner and outer spheres along field lines $A =$ constant. The latter (2.21*d*) is needed to obtain our key second-order differential equation (2.35) for $\mathscr{G}(A)$. Along the polar axis $s = 0$, we must have $B = 0$, which provides the boundary condition

$$\mathscr{G}(0) = 0. \tag{2.22}$$

A second boundary condition is required on the $\mathscr{C}$-line $A = A_c$, which is ultimately determined by matching with the shear-layer that embeds the magnetic field line $\mathscr{C}$.

Significantly, the transverse length scale across the shear-layer on $\mathscr{C}$, though small $O(M^{-1/2})$, is large compared with the Hartmann layer length scale $O(M^{-1})$. Consequently, inside the shear-layer, the contribution $-M^2|\boldsymbol{B}_M|^2 s\Omega$ to the Lorentz force (2.8) is large compared with the viscous force $(\nabla^2 - s^{-2})(s\Omega)$ in (2.7*a*). With the viscous force neglected, the entire Lorentz force (2.8) vanishes,

$$(\nabla\vartheta - \Omega\,\nabla A)\cdot(\nabla A) \approx 0, \tag{2.23a}$$

a result which also holds in the mainstream (see (2.18*a*) and recall that $(\nabla\Phi)\cdot(\nabla A) = 0$). Integration of (2.23*a*) across the shear-layer shows that the electric potential ϑ suffers the jump

$$\Theta_{\mathscr{C}} \equiv \vartheta|_{A\downarrow A_c} - \vartheta|_{A\uparrow A_c} \approx \int_{A\uparrow A_c}^{A\downarrow A_c} \Omega\,\mathrm{d}A \tag{2.23b}$$

in passing from the equatorial region $\mathscr{E}$ to the polar region $\mathscr{P}$. Used in conjunction with (2.4*c*), we may determine the volume flux

$$\mathscr{V}_{\mathscr{C}} \equiv \int_{\mathscr{C}}\int_{A\uparrow A_c}^{A\downarrow A_c} s\Omega\,\mathrm{d}\mathscr{S} \approx \int_{\mathscr{C}} \frac{r\Theta_{\mathscr{C}}}{2\Phi_c}\,\mathrm{d}r \tag{2.23c}$$

(cf. Bühler 2009, equation (42)) carried by the shear-layer, where $\Phi_c(r) \equiv \Phi(r, A_c)$ (see (2.15*b*)).

2.2. *The Hartmann layers*

The determination of the unknown functions $\mathscr{F}$ and $\mathscr{G}$ (also $\mathscr{J} = -\mathscr{G}'$) of A requires knowledge of the jump conditions across the Hartmann layers adjacent to the inner and outer boundaries. The Hartmann layer solution of the governing equations (2.7) appropriate to each of the inner i and outer o boundaries is

$$\Omega \approx \Omega_{(i,o)} + (\varsigma\omega)_{(i,o)} \exp\left[-M\left(\varsigma\,|B_r|\right)_{(i,o)}\left(r - r_{(i,o)}\right)\right], \tag{2.24}$$

where $\Omega_{(i,o)}$, introduced in (2.21*b*,*d*), is the mainstream angular velocity just outside each Hartmann layer and $(\varsigma\,|B_r|)_{(i,o)} \equiv \varsigma_{(i,o)}\,|B_{r(i,o)}|$ and $\omega_{(i,o)} = \varsigma_{(i,o)}(\Omega^S - \Omega)_{(i,o)}$, specifically

$$\omega_i = 1 - \Omega_i, \qquad \omega_o = \Omega_o, \tag{2.25a,b}$$

are the magnitudes of the angular velocity jumps across them; the magnitude of the angular velocity jump across the mainstream is

$$\Omega_i - \Omega_o = 1 - (\omega_i + \omega_o). \tag{2.25c}$$

In the northern hemisphere $z \geqslant 0$, where $B_r = |B_r|$, the Hartmann layer solution (2.24) determines the composite expansions

$$sB \approx -\mathscr{G} + M^{-1}\left(\omega s^2\right)_{(i,o)} \exp\left[-M\left(\varsigma\,|B_r|\right)_{(i,o)}\left(r - r_{(i,o)}\right)\right], \tag{2.26a}$$

$$rs\,j_\theta \approx A\,\mathscr{J} + \left(\varsigma\omega r s^2 B_r\right)_{(i,o)} \exp\left[-M\left(\varsigma\,|B_r|\right)_{(i,o)}\left(r - r_{(i,o)}\right)\right] \tag{2.26b}$$

of the magnetic field B and the tangential component of electric current j_θ, which embed the mainstream solutions (2.17*a*,*c*). For later use, we introduce the local Hartmann numbers $M^{loc}_{(i,o)} = M(r|B_r|)_{(i,o)}$, based on the radial component of magnetic field B_r^* and radius r^* at the inner and outer boundaries. With the help of (2.3*a*) and (2.13*b*), each may be expressed in the form

$$M^{loc}_{(i,o)} \equiv 2M|\Phi_{(i,o)}| = Mr^{-2}_{(i,o)}\sqrt{1 - 2r_{(i,o)}A}. \tag{2.27}$$

The tangential component of electric field $E_\theta = j_\theta - s\Omega B_r$ (see (2.6*c*)) in the Hartmann layers determined upon the substitution of (2.24) and (2.26*b*) is given by

$$rsE_\theta = -s\frac{\partial\vartheta}{\partial\theta} \approx A\,\mathscr{J} - \left(\Omega r s^2 B_r\right)_{(i,o)}, \tag{2.28a}$$

independent of the boundary layer coordinate $M(r - r_{(i,o)})$. When (2.28*a*) is evaluated at the outer edge of the Hartmann layers, the use of (2.2*a*), (2.3*a*) and (2.14*a*–*c*) determines

$$-\left(\frac{E_\theta}{sB_r}\right)_{(i,o)} = \vartheta'_{(i,o)} \approx \Phi'_{(i,o)}\,\mathscr{J} + \Omega_{(i,o)}, \tag{2.28b}$$

consistent with (2.19*a*,*b*). We may interpret the contribution $A\mathscr{J}/(rs)_{(i,o)}$ in (2.28*a*) to $E_{\theta(i,o)}$ as the tangential component of the 'relative' electric field (as measured in the reference frame rotating with the fluid at angular velocity $\Omega_{(i,o)}$). At the boundaries continuity across the solid–fluid interfaces fixes the values inside the solids:

$$E^S_{\theta\,(i,o)} \approx E_{\theta(i,o)}, \qquad \vartheta^S_{(i,o)} \approx \vartheta_{(i,o)}. \tag{2.29a,b}$$

Likewise, with the help of (2.26*a*,*b*), continuity of B and $\sigma^{-1} j_\theta$ (see (2.12*a*)) across the solid–fluid interfaces determines the relations

$$(sB^S)_{(i,o)} \approx -\mathscr{G} + M^{-1}\left(\omega s^2\right)_{(i,o)} = -\mathscr{G} + 2M^{-1}\left(\omega r^3\right)_{(i,o)} A, \tag{2.29c}$$

$$\left(\frac{\sigma}{\sigma^S} rs\, j_\theta^S\right)_{(i,o)} \approx A\,\mathscr{J} + \left(\varsigma \omega r s^2 B_r\right)_{(i,o)} = A\,\mathscr{J} + 4\left(\varsigma \omega r^3 \Phi\right)_{(i,o)} A \tag{2.29d}$$

respectively, where we have made use of (2.13*a*) and (2.14*c*). The values of $(sB^S)_{(i,o)}$ and $(rs\, j_\theta^S)_{(i,o)}$ inside the solids at their surfaces $r = r_{(i,o)}$ are related via the solution of the potential problems (2.11) within the range $0 < \varsigma_{(i,o)}(r - r_{(i,o)}) < \delta_{(i,o)}$.

2.3. *Thin finitely conducting boundaries*

The main obstacle to obtaining analytic solutions of the complete system of governing equations is the necessity of solving the potential problem for the magnetic fields in the solids. For thick shells it is only possible to make progress in certain limiting cases such the case of an insulating outer boundary $\sigma_o^S = 0$ considered by Dormy *et al.* (2002) and the case of perfectly conducting boundaries $\sigma_{(i,o)}^S = \infty$, which we will discuss in § 3. The MHD solutions in the flow region $r_i < r < r_o$ for both of these problems are largely independent of the solid shell width and are equally well described in the thin shell limit

$$\delta_{(i,o)} \ll r_{(i,o)}. \tag{2.30}$$

When this approximation is made for thin boundaries of finite conductivity $\sigma_{(i,o)}^S$ the electric currents in the solids are locally uniform and parallel to the boundaries. The magnitudes of their total electric current flow are determined by the magnetic field jumps across the thin solids. In view of the zero value of B at the solid–vacuum interfaces (see (2.12*b*)), their magnitudes are simply

$$\left(\delta\, j_\theta^S\right)_{(i,o)} \approx -(\varsigma B^S)_{(i,o)} \tag{2.31a}$$

or more usefully

$$\left(\frac{\sigma}{\sigma^S} rs\, j_\theta^S\right)_{(i,o)} \approx -\left(\frac{\varsigma}{\varepsilon}\right)_{(i,o)} (sB^S)_{(i,o)}, \tag{2.31b}$$

where

$$\varepsilon_{(i,o)} \equiv \left(\frac{\sigma^S}{\sigma}\frac{\delta}{r}\right)_{(i,o)} \tag{2.31c}$$

are the relative conductances of the solid shells (see Shercliff 1956; see also Walker 1981). The relation (2.31*b*) may be used in conjunction with the magnetic boundary conditions (2.29*c*,*d*) to determine the magnitude

$$\omega_{(i,o)} = \frac{-\varsigma_{(i,o)}\mathscr{J} + \varepsilon_{(i,o)}^{-1}\mathscr{G}/A}{2r_{(i,o)}^3\left(2\Phi_{(i,o)} + (\varepsilon_{(i,o)}M)^{-1}\right)} \tag{2.32}$$

of the angular velocity jumps across the inner and outer Hartmann layers. The relative size of the two terms $2\Phi_{(i,o)}$ and $(\varepsilon_{(i,o)}M)^{-1}$ is the same as the relative size of the local Hartmann number $M_{(i,o)}^{loc}$ (see (2.27)) and $\varepsilon_{(i,o)}^{-1}$.

In view of the physical interpretation of sB as a measure of the electric current flux across any closed axisymmetric surface, we may define the ratio of the electric current fluxes carried by the inner and outer Hartmann boundary layers equator-ward across the circles $(r_{(i,o)}, A)$ to the total electric current inflow from the the mainstream across

the polar cap bounded by those circles as

$$1 - \mathscr{L}_{(i,o)} \equiv \left(\mathscr{G} + \left(sB^S\right)_{(i,o)}\right) \Big/ \mathscr{G}, \tag{2.33a}$$

where $\mathscr{L}_{(i,o)}$ measures the fraction leaked directly into each solid boundary. Further use of (2.29c) and (2.32) determines the values

$$\mathscr{L}_{(i,o)} = 1 + \frac{\varsigma_{(i,o)}\varepsilon_{(i,o)}(A\mathscr{J}/\mathscr{G}) - 1}{\varepsilon_{(i,o)}M^{loc}_{(i,o)} + 1}, \tag{2.33b}$$

where $M^{loc}_{(i,o)}$ are defined by (2.27).

Inside the equatorial region $\mathscr{E}$, the result (2.20a) states that $\mathscr{G} = 0$ everywhere, implying $\mathscr{J} = 0$ also. Hence it follows from (2.32) that $\omega_i = 0$, whenever $\varepsilon_i > 0$. In turn, this determines $\Omega_i = 1 - \omega_i = 1$ with the consequence (see (2.20c)) that

$$\Omega \approx \mathscr{F} = 1, \qquad sB \approx -\mathscr{G} = 0 \qquad \text{in } \mathscr{E}. \tag{2.34a,b}$$

It means that, when the inner solid shell is electrically conducting, the fluid in the equatorial region $\mathscr{E}$ co-rotates with the inner boundary $r = r_i$, on which the Hartmann layer is absent.

The formulation of the mainstream problem in the polar region $\mathscr{P}$ is completed upon substitution of the values of $\Omega_i - \Omega_o$ and $\omega_{(i,o)}$ given by (2.21d) and (2.32) respectively into $(\Omega_i - \Omega_o) + (\omega_i + \omega_o) = 1$ (see (2.25c)). It yields

$$(\Phi_i - \Phi_o)\,\mathscr{J}' - \frac{\mathscr{J} - \varepsilon_i^{-1}\mathscr{G}/A}{2r_i^3\left(2\Phi_i + (\varepsilon_i M)^{-1}\right)} + \frac{\mathscr{J} + \varepsilon_o^{-1}\mathscr{G}/A}{2r_o^3\left(2\Phi_o + (\varepsilon_o M)^{-1}\right)} = 1, \tag{2.35}$$

which, since $\mathscr{J} \equiv -\mathscr{G}'$, is a second-order ordinary differential equation for $\mathscr{G}(A)$. It must be solved subject to the polar boundary condition $\mathscr{G}(0) = 0$ (see (2.22)) and the appropriate matching condition across the shear-layer on $\mathscr{C}$, which generally is simply $\mathscr{G}(A_c) = 0$ to ensure continuity of B (see (2.34b)). However, in the double limit $\varepsilon_o \ll 1$, $M \gg 1$, the differential equation (2.35) leads to a singular perturbation problem in which a small parameter multiplies the highest derivative $\mathscr{G}''$. Then, as we explain in §§ 4.1 and 4.2, there are two limiting possibilities: for sufficiently large ε_o, matching is achieved by demanding that the solution of (2.35) satisfies $\mathscr{G}(A_c) = 0$, while for sufficiently small ε_o, the second derivative term $\mathscr{G}''$ is negligible throughout the mainstream polar region, and so no boundary condition is imposed.

We may illustrate the latter limiting possibility by the special insulating outer boundary case $\varepsilon_o = 0$ ($\mathscr{L}_o = 0$) considered by Dormy *et al.* (2002). The polar mainstream solution for that case may be recovered from our thin shell equation (2.35) with $\varepsilon_{(i,o)} > 0$, which in the limit $\varepsilon_o \downarrow 0$ yields

$$-sB \approx \mathscr{G} = M^{-1}r_o^2\,(A/A_c) \qquad \text{in } \mathscr{P}, \tag{2.36}$$

showing that $\mathscr{G} = O(M^{-1})$ and $\mathscr{J} = -\mathscr{G}' = O(M^{-1})$. It follows from (2.19$b$) that $\Omega = \mathscr{F}(A) + O(M^{-1})$ in the mainstream, i.e. Ferraro's (1937) law of isorotation holds, while from (2.32) it follows that $1 - \Omega_i = \omega_i = O(M^{-1})$ (also $1 - \mathscr{L}_i = O(M^{-1})$). Since $\mathscr{F}(A) = \Omega_i = 1 + O(M^{-1})$, we deduce that the entire mainstream co-rotates with the inner boundary not only in $\mathscr{E}$ (see (2.34)) but in $\mathscr{P}$ as well (cf. Dormy *et al.* 2002, equation (2.13a)), leaving the angular velocity jump between the inner and outer sphere to be accommodated by the outer Hartmann layer: $\omega_o = 1 + O(M^{-1})$. Solution (2.36) meets the boundary condition $\mathscr{G}(0) = 0$ but takes the approximate non-zero value $\mathscr{G}(A_c) = M^{-1}r_o^2$ at the $\mathscr{C}$-line. The requirement that $\mathscr{G}$ must adjust across the $\mathscr{C}$-line to zero is the *raison d'être* for the shear-layer and the super-rotation in it. A

significant feature of solution (2.36) derived by Dormy *et al.* (2002) for the insulating outer boundary case is the small $O(M^{-1})$ size of $\mathscr{G}$ in $\mathscr{P}$. When both boundaries are conducting, which is the main concern of this paper, $\mathscr{G}$ is relatively large, $O(1)$, in $\mathscr{P}$, and then much stronger super-rotation is achieved in the shear-layer $\mathscr{C}$.

3. Perfectly conducting boundaries of finite thickness

The main objective of this section is to describe analytic and numerical results for finitely conducting thick boundaries. An analytic solution for the mainstream region is possible, when the boundaries are perfect conductors. The case of a perfectly conducting boundary must be interpreted with caution. For if the boundaries are truly perfectly conducting, $1/\sigma^S_{(i,o)} = 0$, the magnetic fields in them are frozen and have no possibility of adjusting to conditions external to the solid conductors. We must therefore consider finite but highly conducting boundaries and consider the limit $\sigma^S \uparrow \infty$ instead. Then over sufficiently long times the magnetic field in them can respond to achieve whatever steady-state field is appropriate; i.e. the length of time required for transients to decay tends to infinity in concert with $\sigma^S_{(i,o)}$.

Despite these cautionary remarks, the perfectly conducting limit is attractive, as Bühler (2009) found too, because relative to the co-rotating frame the solid boundaries support no electric field and are equi-(electric)-potential surfaces in their rotating frames. Since for a sphere rotating with the constant angular velocity unity, we have $\boldsymbol{u} \times \boldsymbol{B}_M = \nabla A$; it follows that

$$\vartheta^S_i = A - A_m, \qquad \vartheta^S_o = 0, \qquad \text{when} \qquad \sigma^S_{(i,o)} \uparrow \infty, \tag{3.1a,b}$$

where the as-yet-unknown constant A_m measures the potential difference between the outer and inner boundaries on the symmetry axis $s = 0$. Since $E^S_{\theta\, i} = (sB_r)_i$, $E^S_{\theta\, o} = 0$ and $\Omega_i = 1 - \omega_i$, $\Omega_o = \omega_o$, it follows that the mainstream 'relative' tangential electric field component $(E_\theta + s\Omega B_r)_{(i,o)}$ is simply $-(\varsigma s\omega B_r)_{(i,o)}$, which, by Ohm's law (2.28*b*), equals the tangential electric current component $\mathscr{J} B_{\theta(i,o)}$. Since $s_{(i,o)}\Phi'_{(i,o)} = -(B_\theta/B_r)_{(i,o)}$ (see (2.3*a*,*b*) and (2.14*b*)), the equality yields

$$\omega_{(i,o)} = \varsigma_{(i,o)}\Phi'_{(i,o)}\mathscr{J}. \tag{3.2}$$

By implication, the vanishing of $\omega_{(i,o)}$ coincides with the vanishing of $\mathscr{J} B_{\theta(i,o)}$. So, whereas our tangential component of the applied magnetic field only vanishes at the poles $A = 0$, in the case of the cylindrical shell geometry of Bühler (2009), his uniform magnetic field was normal to all plane boundaries. Thus Bühler (2009) had no 'relative' tangential electric field at the boundaries with the consequence that there were no Hartmann layers.

Directly, the solution for $\mathscr{G}(A)$ is known, and the magnetic field $B^S_{(i,o)}$ on the surface of the solids is given by the boundary condition (2.29*c*). Then the magnetic field inside the solid conductors, $0 < \varsigma_{(i,o)}(r_{(i,o)} - r) < \delta_{(i,o)}$, is determined by the solutions of (2.11). We stress that result (3.2) is independent of the solid widths $\delta_{(i,o)}$ and, in particular, is given by our thin shell boundary result (2.32) with $\varepsilon^{-1}_{(i,o)} \uparrow \infty$. These simplifications allow us to develop the analytic theory of § 3.1 below, which is supported by the full numerical integration of the governing equations (2.7*a*,*b*). The shear-layer theory connecting the polar and equatorial mainstream regions is developed in § 3.3, and numerical solutions of the shear-layer equations are described in § 3.4.

To test the sensitivity of the results to the perfectly conducting boundary approximation, we report in § 3.2 numerical results for the case in which the entire

space outside the fluid is occupied by rigid solids ($r_i - \delta_i = 0$, $r_o + \delta_o \to \infty$) with the same electrical conductivity as the fluid ($\sigma^S_{(i,o)} = \sigma$).

All numerical results reported in this section are for the particular case

$$r_i = 4, \qquad r_o = 5, \qquad \zeta_i \,(\equiv r_i/r_o) = 0.8, \tag{3.3a,b,c}$$

$$A_c \equiv 1/2r_o = 0.1. \tag{3.3d}$$

Other parameters β_i, α_i dependent on ζ_i (see (B 2*c*,*d*)), which we need, take the values

$$\beta_i = 5^{3/2}/2^5 \approx 0.3494, \qquad \alpha_i = 6/5^{3/2} = 0.5367. \tag{3.4a,b}$$

3.1. *The mainstream solution*

In the perfectly conducting boundaries limit

$$\varepsilon_{(i,o)} \uparrow \infty, \tag{3.5}$$

the mainstream solution (2.20*b*,*c*) in the equatorial region $\mathscr{E}$ is completed upon the use of $\mathscr{T}' = \mathscr{F} = 1$ (see (2.34*a*)) and application of the inner boundary condition (3.1*a*). They give $\mathscr{T} = A - A_m$, which together with $\mathscr{G} = 0$ (see (2.34*b*)) determine

$$\vartheta = A - A_m, \qquad \Omega = 1, \qquad B = 0 \qquad \text{in} \quad \mathscr{E}. \tag{3.6a,b,c}$$

For the polar region $\mathscr{P}$, substitution of $\vartheta_{(i,o)} = \vartheta^S_{(i,o)}$ (see (2.29*b*)) given by (3.1*a*,*b*) into (2.21*a*) determines

$$\vartheta = \begin{cases} A - A_m + (\Phi - \Phi_i)\,\mathscr{J}, \\ (\Phi - \Phi_o)\,\mathscr{J}, \end{cases} \tag{3.7a,b}$$

whose equivalence shows that

$$(\Phi_i - \Phi_o)\,\mathscr{J} = A - A_m. \tag{3.8}$$

Evidently, the magnetic field line $A = A_m$ is significant because on it the mainstream electric current $\mathscr{J}\boldsymbol{B}_M$ (see (2.17*b*)) vanishes. Finally, upon substitution of the values of $\Omega_{(i,o)}$ determined by (2.25*a*,*b*) and (3.2), the angular velocity Ω in the polar region $\mathscr{P}$ given by (2.21*b*) becomes either of the following two forms:

$$\Omega = \begin{cases} 1 - (\Phi_i \mathscr{J})' + \Phi\,\mathscr{J}', \\ -(\Phi_o \mathscr{J})' + \Phi\,\mathscr{J}'. \end{cases} \tag{3.9a,b}$$

Their equivalence shows that $[(\Phi_i - \Phi_o)\mathscr{J}]' = 1$, which is the differential equation (2.35) for our case of perfectly conducting boundaries and for which (3.8) is the integral. We may illustrate these polar region results by applying them to the uniform magnetic field case $A = (1/2)s^2$, $\Phi = -z$ of Bühler (2009) for the flow between cylindrical shells. Upon making the change of variables $\mathscr{J} \to j_z$, $A_m \to -\phi_0$, $\vartheta \to \phi$, $s\Omega \to v$ and $s \to r$ and adopting his value $\phi_0 = -1/4$, our formulae (3.8), (3.7*b*) and (3.9*b*) determine his results (26), (20) and (24) respectively for the flow in the region $r < 1$ above his inner cylinder.

To complete the specification of our polar problem, we require the solution $\mathscr{G}(A)$ of $\mathscr{G}' = -\mathscr{J}$, where $\mathscr{J}$ is given by (3.8), which vanishes on the symmetry axis $A = 0$ and at the $\mathscr{C}$-line $A = A_c$:

$$\mathscr{G}(0) = \mathscr{G}(A_c) = 0. \tag{3.10}$$

The analytic solution of this problem, which also determines A_m, is given in Appendix A. Of particular interest is the value of $\mathscr{J}$ at A_c determined by (3.8). Noting that

$\Phi_o(A_c)=0$, it is

$$\mathscr{J}_c = (A_c - A_m)/\Phi_Q, \tag{3.11}$$

where $\Phi_Q \equiv \Phi_i(A_c)$ (see (2.15c)). The explicit value of $\mathscr{J}_c \equiv \mathscr{J}(A_c)$ is given by (A 5) in Appendix A. Further, the use of the equatorial and polar values (3.6a) and (3.7a) of ϑ on the $\mathscr{C}$-line determines the electric potential jump (2.23b). It is

$$\Theta_{\mathscr{C}} = (\Phi_Q - \Phi_c)\,\mathscr{J}_c, \tag{3.12a}$$

which, in turn using (2.23c), determines the volume flux carried by the shear-layer:

$$\mathscr{V}_{\mathscr{C}} = \Xi\,\mathscr{J}_c, \qquad \text{where} \qquad \Xi \equiv \frac{1}{2}\int_{r_i}^{r_o}\left(\frac{\Phi_Q}{\Phi_c}-1\right) r\,\mathrm{d}r \tag{3.12b}$$

is a line integral along $\mathscr{C}$. The explicit values of $\mathscr{J}_c$ and Ξ are given by (A 5) and (B 5) respectively.

To appreciate the divergent nature of the angular velocity Ω in the vicinity of the $\mathscr{C}$-line, we note that Φ_o' determined by (2.13b) and (2.14b) may be written in the form

$$\Phi_o' = -A_c^{3/2}(A_c - A)^{-1/2}. \tag{3.13}$$

So, as $A \uparrow A_c$, the derivative of (3.8) yields the divergent asymptotic behaviour $\mathscr{J}'/\mathscr{J}_c \approx \Phi_o'/\Phi_Q$, since $\Phi_o(A_c)=0$. Used in conjunction with (3.9a), this result establishes the divergent form $\Omega - 1 \approx -\Theta_{\mathscr{C}}(\mathscr{J}'/\mathscr{J}_c)$, in which $\Theta_{\mathscr{C}}$ is given by (3.12a). The asymptotic behaviour of B follows from (2.17a) and (3.10). The results so obtained are

$$\left.\begin{aligned} sB &\approx -\mathscr{J}_c(A_c - A), \\ \Omega - 1 &\approx A_c^{3/2}(\Theta_{\mathscr{C}}/\Phi_Q)(A_c - A)^{-1/2} \end{aligned}\right\} \qquad \text{as} \quad A \uparrow A_c. \tag{3.14a,b}$$

They are needed to provide the boundary conditions on the shear-layer problem.

The fact that $B=0$ on both the axis of symmetry $A=0$ and the the $\mathscr{C}$-line $A=A_c$ (see (3.10)) means that all electric current following the magnetic field lines $A=$ constant in the fluid flows inwards in the region $0 < A < A_m$, where $\mathscr{J} < 0$, and returns outwards in the region $A_m < A < A_c$, where $\mathscr{J} > 0$. This is illustrated in figure 2 (bottom left) for data (3.3) and (3.4a), which by the results of Appendix A determines

$$\varpi_m \equiv A_m/A_c \approx 0.5065, \qquad \text{giving} \qquad \mathscr{J}_c \approx 1.7657 \tag{3.15a,b}$$

(see (A 1c) and (A 5)). To complete this current circuit, almost all the electric current returns in the solids. Only a relatively small fraction $1 - \mathscr{L}_{(i,o)} = O(M^{-1})$ is returned in the Hartmann layers (see (2.33a,b)). Note that the maximum of $-sB$ occurs on the field line $A=A_m$, where $\mathscr{J}=0$. In view of (3.2), the angular velocity jumps $\omega_{(i,o)}(A_m)$ also vanish implying that $\Omega_i(A_m)=1$ and $\Omega_o(A_m)=0$. Elsewhere, the angular velocity jump across the inner and outer Hartmann layers defined by (3.2) determine $\Omega_i(=1-\omega_i)=1-\Phi_i'\mathscr{J}$ and $\Omega_o(=\omega_o)=-\Phi_o'\mathscr{J}$ respectively, in which $\Phi_{(i,o)}' < 0$ (see (2.13b) and (2.14b)). So at the points of intersection of a field line $A=$ constant with the inner and outer boundaries, we have $\Omega_i < 1$, $\Omega_o < 0$ for $0 < A < A_m$ and $\Omega_i > 1$, $\Omega_o > 0$ for $A_m < A < A_c$. The corresponding contours $\Omega =$ constant are illustrated in figure 2 (top left). Interestingly, the super-rotation $1 < \Omega$ (solid) begins in the mainstream, though it increases by an order of magnitude in the shear-layer. On increasing latitude there is a region in which $0 < \Omega < 1$ (dotted). Finally there is a region adjacent to the outer boundary, containing the polar axis of reverse rotation,

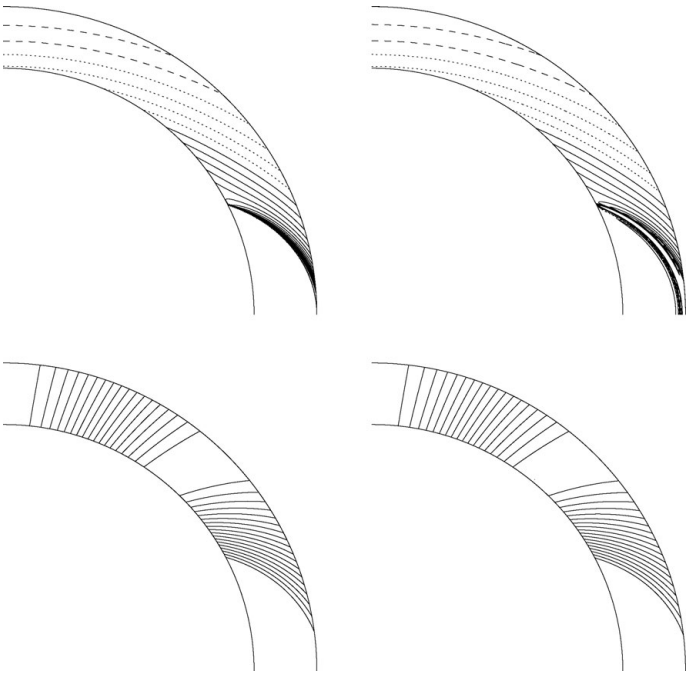

FIGURE 2. Case (3.3), $r_i = 4$, $r_o = 5$ ($\zeta_i = 4/5$); $\sigma^S_{(i,o)} \uparrow \infty$: contours of constant Ω (top row) and sB (bottom row) in the meridional plane for the asymptotic solution (left column) and the full solution at $(2\mathscr{M} \equiv) M/r_o^2 = 10^5$ (right column). In the top row, the contours are drawn dashed for $\Omega < 0$, dotted for $0 < \Omega < 1$ and solid for $\Omega > 1$. In the top right figure, the contour lines are only drawn up to two thirds of the peak value to reduce cluttering in the vicinity of the $\mathscr{C}$-line. In the bottom row, the solid contours all correspond to negative values of sB.

where $\Omega < 0$ (dashed). The actual values of the angular velocity jumps $\omega_{(i,o)}$ across the inner and outer Hartmann layers and $\Omega_i - \Omega_o$ across the mainstream are plotted versus A in figure 3.

The results from the solution of the complete system of partial differential equations (2.7*a*,*b*) at $(2\mathscr{M} \equiv) M/r_o^2 = 10^5$ (see (2.5)) again for the boundary radii (3.3*a*,*b*) are illustrated in the two right-hand portraits in figure 2. Plots of $-sB$ versus A at $r = (r_i + r_o)/2$ for various values of M are illustrated on figure 4 and are compared with the asymptotic formula (A 1*a*) for $-sB = \mathscr{G}(A)$ given in Appendix A. The agreement of the asymptotics with the numerics at $2\mathscr{M} = 10^5$ for figures 2 and 4 is most reassuring.

3.2. *Numerical solutions for finitely conducting boundaries*

The numerical solution of the full governing equations (2.7*a*,*b*), for the case of perfectly conducting boundaries just reported at the end of § 3.1 and those we report here in this section for the case of finitely conducting boundaries, $\sigma^S_{(i,o)} = \sigma$, filling all space exterior to the fluid ($r_i - \delta_i = 0$, $r_o + \delta_i \to \infty$, again using data (3.3)), were obtained using the code introduced by Dormy *et al.* (1998). The computational approach relies on a poloidal-toroidal decomposition of all vector fields. A pseudo-spectral algorithm with a spherical harmonic decomposition is used in θ and ϕ and coupled with a finite-difference method on a stretched grid in the radial direction. Time dependance is reintroduced in (2.7*a*) but not in (2.7*b*) which is solved for exactly at each time step. This procedure leads to faster convergence to the steady state than would be

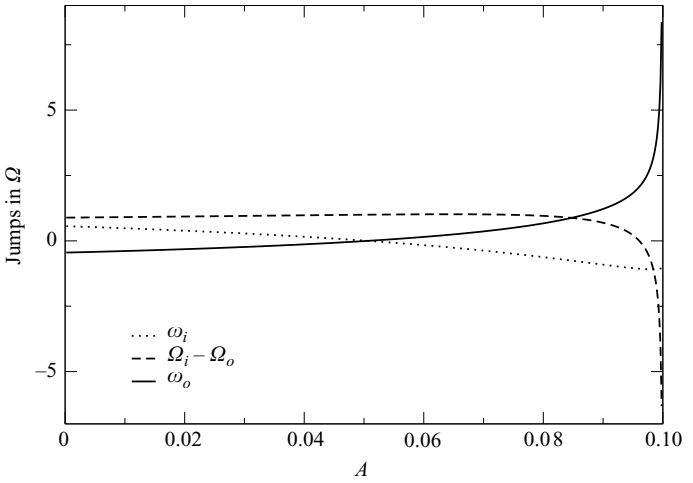

FIGURE 3. Case (3.3), $\zeta_i = 4/5$; $\sigma^S_{(i,o)} \uparrow \infty$: contributions to the jump in Ω across the shell following an imposed field line as a function of A on the range $0 \leqslant A \leqslant A_c = 0.1$, as determined by the asymptotic solution. They are ω_i (dotted) across the inner Hartmann layer, $\Omega_i - \Omega_o$ (dashed) across the the mainstream and ω_o (solid) across the outer Hartmann layer. The total jump $\omega_i + (\Omega_i - \Omega_o) + \omega_o$ is unity (see (2.25c)).

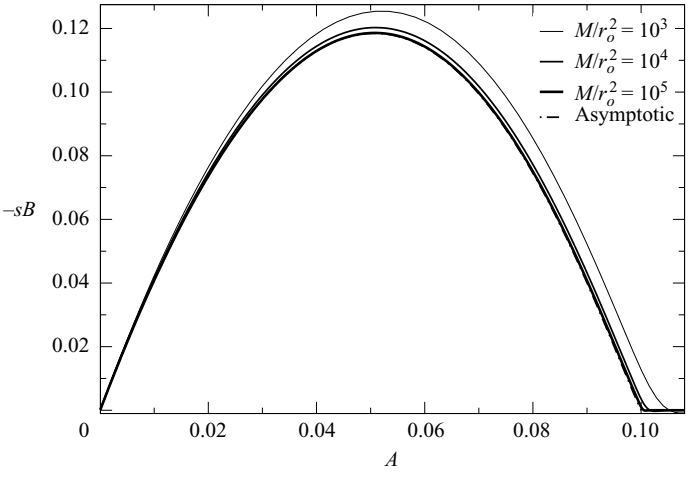

FIGURE 4. Case (3.3), $\zeta_i = 4/5$; $\sigma^S_{(i,o)} \uparrow \infty$: comparison of the current fluxes $-sB$ at mid-radius $r = (r_i + r_o)/2$ plotted versus A, as determined by the full numerics for various values of $2\mathscr{M} \equiv M/r_o^2$, with the asymptotic mainstream value $\mathscr{G}(A)$. To graph plotting accuracy the curve for the highest Hartmann number $2\mathscr{M} = 10^5$ numerical results for $-sB$ coincides with the asymptotic curve $\mathscr{G}(A)$.

achieved by considering the full time dependence in both (2.7a) and (2.7b), because it filters out Alfvén waves.

For our finitely conducting boundaries, the meridional current again largely follows the meridional applied magnetic field lines. Thus contours of constant sB resemble those in figure 2, and so we refrain from plotting them again. On the other hand, though contours of constant Ω for the case of perfectly conducting boundaries (see the upper right portrait of figure 2) and the case of finitely conducting boundaries

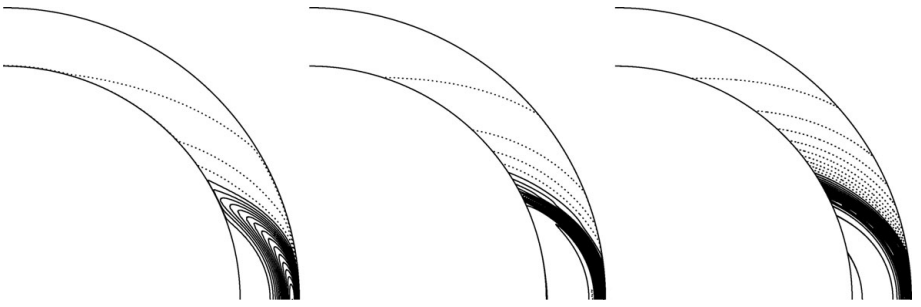

FIGURE 5. Case (3.3), $\zeta_i = 4/5$; $\sigma^S_{(i,o)} = \sigma$: as in figure 2 (top row, right column), contours of constant Ω ($0 < \Omega < 1$, dotted; super-rotation, $1 < \Omega$, solid) for the case of solid boundaries having the same electrical conductivity as the fluid; from left to right $(2\mathscr{M} \equiv) M/r_o^2 = 10^3, 10^4, 10^5$ respectively. Note the absence of reverse flow, $\Omega < 0$, present in the case of perfectly conducting boundaries, identified by the dashed lines in figure 2.

illustrated in figure 5 for various values of large M are qualitatively similar, there are some quantitative differences; e.g. the range of Ω is not as big in the latter conducting case. This fact is partly evidenced by the absence in figure 5 of the reverse rotation (i.e. $\Omega < 0$) visible in figure 2.

3.3. *The shear-layer on* $\mathscr{C}$

In order to understand the nature of the shear-layer on $\mathscr{C}$, we introduce the Shercliff (1953) variables $L^* \Omega_i^{S*} M^{1/2} V_\pm \equiv s^* \Omega^* \pm (\eta/\nu)^{1/2} B^*_\phi / \sqrt{\rho \mu_0}$, with

$$V_\pm = M^{-1/2} s\Omega \pm M^{1/2} B, \tag{3.16}$$

in which the choice of scale factor $M^{1/2}$ is guided by asymptotic behaviours (3.14*a*,*b*) of the mainstream solution in the vicinity of the $\mathscr{C}$-line. The variables Ω and B satisfy (2.7*a*,*b*), when

$$\boldsymbol{B}_M \cdot \nabla V_\pm \pm M^{-1}(\nabla^2 - s^{-2}) V_\pm = s^{-1} B_s V_\mp, \tag{3.17}$$

where $B_s \equiv \boldsymbol{B}_M \cdot \nabla s$ is the s-component of $\boldsymbol{B}_M$. These should be interpreted as advection–diffusion equations, which are coupled by the source terms on their right-hand sides. The advection is manifest by $\boldsymbol{B}_M$; when $\boldsymbol{B}_M$ is directed from the inner to the outer sphere, V_+ (V_-) is convected inwards (outwards). As a consequence, V_+ (V_-) is continuous across the Hartmann layer on the outer (inner) sphere, as implied by (2.24) and (2.26*a*).

Our analytic formulation of the shear-layer problem parallels the earlier development of Dormy *et al.* (2002). The appropriate measure of distance l from Q along the $\mathscr{C}$-line $A = A_c$ is weighted by $s_c^2 |\boldsymbol{B}_M|$ ($s_c = s(r, A_c)$) and defined by (B 3) of Appendix B. The weighted distance normal to $\mathscr{C}$ is measured by the stretched magnetic flux coordinate

$$n \equiv (A_c - A)/\Delta_{\mathscr{C}}, \qquad \text{where} \qquad \Delta_{\mathscr{C}} \equiv \sqrt{\alpha_i / 2M} \tag{3.18a,b}$$

is the shear-layer A-scale. Our choice of sign in the definition of n ensures that n is positive in $\mathscr{P}$ and negative in $\mathscr{E}$. From definition (2.2*a*) of A, we note that the field line $A = A_{\mathscr{C}} \equiv A_c - \Delta_{\mathscr{C}}$ intersects the outer sphere at $(s, z) \approx (r_o, \delta_{\mathscr{C}})$, where

$$\delta_{\mathscr{C}}/r_o = (\Delta_{\mathscr{C}}/A_c)^{1/2} = (\alpha_i/\mathscr{M})^{1/4}, \tag{3.19}$$

in which $\mathscr{M} \equiv M/2r_o^2$ is the equatorial Hartmann number (see (2.5)). Relative to the boundary layer coordinates (l, n), the boundary layer approximations of (3.17) yield

$$\frac{\partial V_\pm}{\partial l} \pm \frac{\partial^2 V_\pm}{\partial n^2} = \frac{1}{s_c}\frac{\mathrm{d}s_c}{\mathrm{d}l} V_\mp, \tag{3.20}$$

where the value of $s_c^{-1}\mathrm{d}s_c/\mathrm{d}l$ is given by (B 4*a*).

Expressed in our boundary layer coordinates, the asymptotic form (3.14*a*,*b*) of the polar mainstream solutions, valid as $A \uparrow A_c$, determines the asymptotic behaviours $M^{1/2}B \approx -\mathscr{J}_c\sqrt{\alpha_i/2}\, s_c^{-1} n$ and $M^{-1/2}s\Omega = O(M^{-1/4}n^{-1/2})$ as $n \uparrow \infty$. These estimates show that the larger size of $M^{1/2}B$ controls the magnitude $V_\pm = O(1)$ of the shear-layer solution. The asymptotic behaviours mentioned together with the equatorial mainstream solution (3.6*b*,*c*) determine the boundary conditions

$$V_\pm \to \begin{cases} \mp \mathscr{J}_c \sqrt{\alpha_i/2}\; s_c^{-1}\, n \;+\; O\big(M^{-1/4}n^{-1/2}\big) & \text{as} \quad n \uparrow \infty, \\ 0 & \text{as} \quad n \downarrow -\infty \end{cases} \tag{3.21}$$

for $0 < l < 1$ in the shear-layer equation (3.20).

Since the solution determines small $O(M^{-1/2})$ magnetic fields $B = M^{-1/2}(V_+ - V_-)/2$ and large differential rotation $\Omega = M^{1/2}(V_+ + V_-)/(2s)$, the Hartmann jump conditions across the inner and outer spheres require the large $O(M^{1/2})$ differential rotation to be reduced to an order-unity value, implying $V_+ = -V_- + O(M^{-1/2})$ at the endpoints $l = 0,\ 1$. On the equator the symmetry condition $B = 0$ gives $V_+ = V_-$. So, in summary, the endpoint boundary conditions on the solution of (3.20) are

$$V_+ = \begin{cases} -V_- & \text{at} \quad \begin{cases} l = 0 & \text{and} \\ l = 1 & \text{for} \quad n > 0, \end{cases} \\ V_- & \text{at} \quad l = 1 \quad \text{for} \quad n < 0. \end{cases} \tag{3.22}$$

In view of (3.6*a*) we express the electric potential ϑ in the shear-layer in the form

$$\vartheta = A_c - A_m + \Theta, \tag{3.23a}$$

where, by (2.23*a*), $\Theta(l, n)$ satisfies

$$\frac{\partial \Theta}{\partial n} = -\Delta_{\mathscr{C}}\Omega \qquad \text{with} \qquad \Theta \to \begin{cases} -\Theta_{\mathscr{C}} & \text{as} \quad n \uparrow \infty, \\ 0 & \text{as} \quad n \downarrow -\infty \end{cases} \tag{3.23b,c}$$

(cf. Bühler 2009, equation (30)), in which, from (2.23*b*),

$$\Theta_{\mathscr{C}} = \Delta_{\mathscr{C}} \int_{-\infty}^{\infty} \Omega \,\mathrm{d}n = \sqrt{\frac{\alpha_i}{2}} \int_{-\infty}^{\infty} \frac{V_+ + V_-}{2s_c}\,\mathrm{d}n. \tag{3.24a}$$

Differentiation of $\Theta_{\mathscr{C}}$ and use of the shear-layer equation (3.20) and boundary conditions (3.21) and (3.22) determines

$$\frac{\mathrm{d}\Theta_{\mathscr{C}}}{\mathrm{d}l} = \frac{\alpha_i}{2}\frac{\mathscr{J}_c}{s_c^2} = -\frac{\mathrm{d}\beta}{\mathrm{d}l}\frac{\mathscr{J}_c}{r_o^2} \qquad \text{with} \qquad \Theta_{\mathscr{C}}(0) = 0, \tag{3.24b,c}$$

where we have made use of (B 4*b*). Integration of (3.24*b*) subject to (3.24*c*) gives

$$\Theta_{\mathscr{C}} = r_o^{-2}(\beta_i - \beta)\,\mathscr{J}_c, \tag{3.24d}$$

which on use of (B 2*a*) agrees with (3.12*a*). Together (3.24*a*,*d*) provide an integral property of the solution of the shear-layer equation (3.20) subject to the boundary conditions (3.21) and (3.22).

The application of the Hartmann jump condition on the outer sphere warrants closer inspection. In terms of the boundary layer coordinates the outer boundary in the vicinity of E_0 ($(l, n) = (1, 0)$) is located at $n = n_o(l) \approx \alpha_i^{3/2} \mathscr{M}^{1/2}(1 - l)^2$ (see Dormy *et al.* 2002, equation (3.8)), which lies within the shear-layer $n = O(1)$, when $|1 - l| = O(M^{-1/4})$. On it, the Hartmann jump condition (3.2) becomes

$$\frac{\partial}{\partial n}(V_+ - V_-) = -2\alpha_i^{3/4} \mathscr{M}^{1/4} n^{1/2}(V_+ + V_-) \qquad \text{for} \qquad n > 0. \tag{3.25}$$

Provided that $n \gg M^{-1/6}$, we can legitimately make the approximation $V_+ + V_- = 0$ used in (3.22). As n is decreased the left- and right-hand sides of (3.25) become of comparable size when $n = O(M^{-1/6})$. This determines the extent of the equatorial Hartmann layer, which has small latitudinal length $z = O(M^{-1/3}) \ll \delta_{\mathscr{C}} = O(M^{-1/4})$ and radial thickness $r_o - r = O(M^{-2/3})$ (see Dormy *et al.* 2002, figure 7). However, inside the equatorial Hartmann layer, another boundary layer problem needs to be solved and the jump condition (3.25) no longer applies. Dormy *et al.* (2002) formulated and solved the equatorial Hartmann layer problem for the case of an insulating boundary, on which the magnetic field B vanishes: $V_+ - V_- = 0$. The solution built on the pioneering study by Roberts (1967*b*) of circular pipe flow in the presence of a uniform transverse magnetic field. There is, however, an important distinction between the Roberts problem, for which the uniform magnetic lines crossing the plane of symmetry intersect the outer boundary, and our problem, for which the dipolar magnetic field lines crossing the equatorial plane peel away from the boundary to trigger the shear-layer. This geometrical difference leads to dynamical differences that are manifest in the respective solutions of the two problems. Despite these essential differences, we refer to the equatorial Hartmann layer as a Roberts layer. Unfortunately, in our perfectly conducting case, we require the electric current j_θ to vanish instead: $\partial(V_+ - V_-)/\partial n = 0$. Though the vanishing of the rotation rate Ω on the boundary ($V_+ + V_- = 0$) is the same for both problems, the difference of the magnetic boundary conditions appears to render the analytic solution of our perfectly conducting case intractable.

Finally, the error estimates stemming from matching to the polar mainstream (3.21) and to the Roberts layer (hinted at by (3.25)) consistently show that the $O(1)$ solution for $V_\pm$ will have errors $O(M^{-1/4})$.

3.4. *Numerical solution of the shear-layer equations*

The numerical solution of (3.20) for data (3.3), (3.4) and (3.15) was implemented by use of an up-wind operator to stabilize the advection term as in Dormy *et al.* (2002). The main difference between the present problem and that relevant to the case of the insulating outer boundary resides in the forcing of this shear-layer via the boundary conditions. Whereas the solution of the shear-layer equation (3.20) in the case of the insulating outer boundary is driven from the equator ($l = 1$) and advected along the shear-layer, the solution in the present case of perfectly conducting boundaries is driven by magnetic sources in the polar mainstream region, which diffuse from $n \uparrow \infty$ (see (3.21)) inwards across the shear-layer. As a consequence, the explicit relaxation procedure introduced in Dormy *et al.* (2002) only converges very slowly for the present problem. So though successive iterations of (3.20) for V_+ and V_- were undertaken as in Dormy *et al.* (2002), the equation for V_+ was relaxed, whereas that for V_- was solved explicitly using the Thomas algorithm (i.e. inverting the tri-diagonal matrix resulting from the second-order operator in n and the diagonal part of the up-winded advection term). This algorithm yielded rapidly convergent solutions.

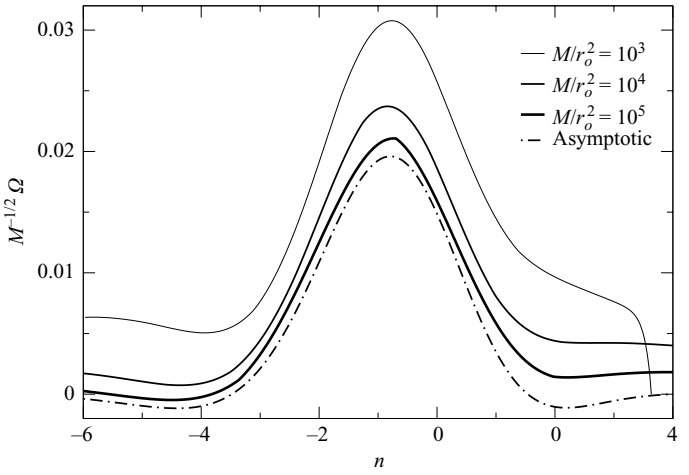

FIGURE 6. Case (3.3), $\zeta_i = 4/5$; $\sigma^S_{(i,o)} \uparrow \infty$: the asymptotic shear-layer solution (dot-dashed curve) compared with the full numerics across the shear-layer along the straight line normal to the $\mathscr{C}$-line at $l = 0.4$. Distance along the straight line is measured by the coordinate n, which measures flux, $A_c - A$, stretched by the factor $\Delta_{\mathscr{C}}^{-1} \propto M^{1/2}$ (see (3.18)). The values of $M^{-1/2}\Omega$ for various values of $2\mathscr{M} \equiv M/r_o^2$, as determined by the full numerics, are illustrated by the continuous curves. In the $2\mathscr{M} = 10^5$ case, the outer boundary is reached at $n = n_o$ (say) < 4 short of the right-hand edge of the figure. In the vicinity $n_o - n = O(M^{-1/2}) > 0$ of the outer boundary, the abrupt drop in the curve is a manifestation of the Hartmann layer; the magnitude of the drop of $M^{-1/2}\Omega$ is $M^{-1/2}\omega_o$.

From the numerical solution of the complete governing equations (2.7) for the same data (3.3), the values of $M^{-1/2}\Omega$ are plotted versus n along the straight line normal to the $\mathscr{C}$-line at $l = 0.4$ on figure 6 for various values of M. They are compared with the numerical solution $M^{-1/2}\Omega = (V_+ + V_-)/2s_c$ of the shear-layer equation (3.20). A similar plot is given on figure 7 at $l = 1$, for which the straight line normal to the $\mathscr{C}$-line is the normal to the outer sphere at E_o directed inwards along the equatorial plane. Figures 6 and 7 show satisfactory convergence with increasing M, comparable to that found by Dormy *et al.* (2002) for insulating boundaries. Nevertheless, corrections obtained from the solution of the equatorial boundary layer problem ought to improve convergence in figure 7 (cf. Dormy *et al.* 2002, figure 9), but unfortunately, as explained at the end of § 3.3, the analytic solution of that problem subject to the perfect conductor boundary condition (3.22) at $l = 1$ is not available to us.

4. Thin shell outer boundary of finite conductivity

Previous MHD Couette flow studies, such as those of Dormy *et al.* (2002), Hollerbach *et al.* (2007), Mizerski & Bajer (2007) and Bühler (2009), have considered an inner conducting boundary, and so in this section we do the same. Our ultimate aim (see § 5) is to compare our asymptotic predictions of the super-rotation rate in the shear-layer with the numerical results of Mizerski & Bajer (2007) (see § 5.1) and those of Hollerbach *et al.* (2007) for the case of an inner solid sphere, $r_i - \delta_i = 0$, possessing the same electrical conductivity as the fluid, $\sigma_i^S = \sigma$ (see § 5.2). However, our numerical comparisons in §§ 3.1 and 3.2 of the respective cases of inner perfectly and finitely, $\sigma_i^S = \sigma$, conducting boundaries revealed that the qualitative nature of the

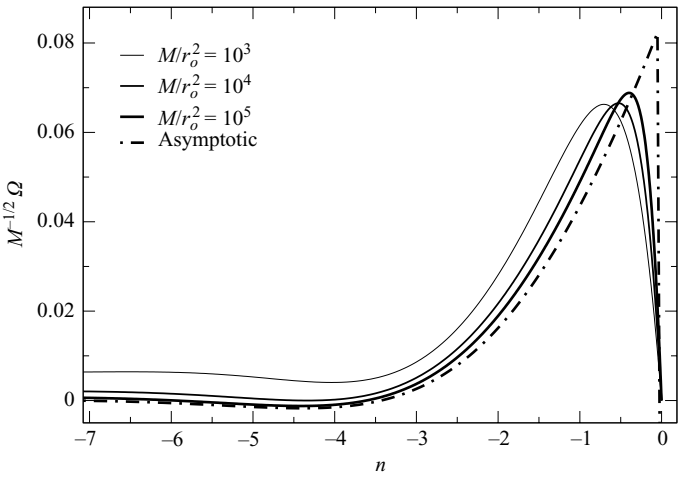

FIGURE 7. Case (3.3), $\zeta_i = 4/5$; $\sigma^S_{(i,o)} \uparrow \infty$: as in figure 6 but at $l = 1$, where the straight line normal to the $\mathscr{C}$-line lies in the equatorial plane. The shear-layer solution V_+/r_o (dot-dashed curve) is compared with the full numerical solutions $M^{-1/2}\Omega$ (continuous curves).

solutions are similar. Therefore, we simplify matters in this section and the following section, § 5.1, by restricting attention to the perfect conductivity limit

$$\sigma_i^S \uparrow \infty, \qquad \varepsilon_i \uparrow \infty. \tag{4.1}$$

Like Hollerbach *et al.* (2007), we consider a thin outer shell and investigate the nature of the solution for various values of the relative conductance ε_o.

So far we have solutions in two limiting cases. The first is that of an insulating outer boundary $\varepsilon_o = 0$ investigated by Dormy *et al.* (2002), for which the electric current flow is returned at the outside entirely within the outer Hartmann layer rather than within the solid bounding shell ($\mathscr{L}_o = 0$). The second is that of a perfectly conducting outer boundary $\varepsilon_o \uparrow \infty$, studied in § 3, for which the electric current flow is returned largely within the outer solid instead ($1 - \mathscr{L}_o = O(M^{-1})$). Since electric current is unable to leak into the solid, in the former insulating case, a Hartmann layer on the outer boundary is readily supported which accommodates the entire angular velocity jump between the inner and outer spherical boundaries. The fact, however, that $-sB = \mathscr{G} \approx M^{-1} r_o^2 (A/A_c)$ in the polar region $\mathscr{P}$ (see (2.36)) means that the electric current, though small, flows outward throughout the polar region and has to return entirely within the shear-layer, so causing the super-rotation. In contrast, in the latter perfectly conducting case, the bulk of the current flow returns within the mainstream polar region $\mathscr{P}$. Nevertheless, because the current flows involved are so large, what remains to flow along the $\mathscr{C}$-line shear-layer is still able to drive the super-rotation in it, which is even stronger than for the former insulating case.

Our objective here is to understand the transition between the two limiting cases. It turns out, from a physical point of view, that the distinguishing feature is whether the return current flow is predominantly in the mainstream as in the $\varepsilon_o \uparrow \infty$ case, or in the $\mathscr{C}$-line shear-layer as in the $\varepsilon_o = 0$ case; i.e. put mathematically, can we apply the mainstream boundary condition $\mathscr{G}_c = 0$ or not? Since this distinction depends on the nature of the solution close to the $\mathscr{C}$-line, which is particularly sensitive to the Hartmann layer near the equator E_o to the outer boundary, we often find it helpful to use the equatorial Hartmann number $\mathscr{M}$ (see (2.5)) based on conditions there.

Finally, since we wish to compare our results with those of Hollerbach *et al.* (2007) (see particularly § 5.2), all the numerical results presented in this section and the following section, § 5, are for the particular case in which

$$r_i = 1, \qquad r_o = 2, \qquad \zeta_i = 0.5, \tag{4.2a,b,c}$$

$$A_c \equiv 1/2r_o = 0.25. \tag{4.2d}$$

With $\zeta_i = 0.5$, (B 2*c*,*d*) determine the parameter values

$$\beta_i = \sqrt{2} \approx 1.4142, \qquad \alpha_i = 3/2^{3/2} \approx 1.0607. \tag{4.3a,b}$$

4.1. *The large-Hartmann-number limit*

Under the assumption, that

$$M \uparrow \infty \tag{4.4}$$

with $\varepsilon_i \uparrow \infty$ (see (4.1)), the electric potential continues to be given everywhere in the mainstream by

$$\vartheta = A - A_m + (\Phi - \Phi_i)\mathscr{J} \tag{4.5}$$

(see (3.7*a*)). With $\varepsilon_o = O(1)$, the angular velocity jumps (2.32), upon use of (2.14*b*), become

$$\omega_i = \Phi_i'\mathscr{J}, \qquad \Omega_o = \omega_o = -\Phi_o'(\mathscr{J} + \varepsilon_o^{-1}\mathscr{G}/A), \tag{4.6a,b}$$

which differs from (3.2) only through the addition of the extra term $-\varepsilon_o^{-1}\Phi_o'\mathscr{G}/A$ in (4.6*b*). Its presence can be traced to the fact that the tangential electric field $(j_\theta^S/\sigma^S)_o = -\mathscr{G}/(s\delta\sigma^S)_o$ (see (2.29*c*) and (2.31*a*)) in the outer solid is finite, rather than zero as it was in the perfectly conducting case, so altering the angular velocity jump across the outer Hartmann layer determined by (2.29*d*). However, like in the perfectly conducting case, we have ignored the electric current carried by the outer Hartmann layer, as signalled by the neglect of the $O(M^{-1})$ term in (2.29*c*), which vanishes in the limit $M \uparrow \infty$.

With the angular velocity jumps (4.6*a*,*b*), the mainstream equation (2.35) reduces to

$$[(\Phi_i - \Phi_o)\mathscr{J}]' - \varepsilon_o^{-1}\Phi_o' A^{-1}\mathscr{G} = 1 \qquad \text{with} \qquad \mathscr{G}' = -\mathscr{J}, \tag{4.7a,b}$$

where Φ_i and Φ_o are defined by (2.13*b*). We have solved (4.7) subject to the boundary conditions $\mathscr{G}(0) = 0$, $\mathscr{G}(A_c) = 0$ for the sphere radii (4.2*a*,*b*) and have illustrated our results for various values of ε_o by plots of $\mathscr{J}/\varepsilon_o$ and Ω_o versus A over the range $0 \leqslant A \leqslant A_c$ in figures 8(*a*) and 8(*b*) respectively. In addition, since the value of $\mathscr{J}_c \equiv \mathscr{J}(A_c)$ on the $\mathscr{C}$-line determines the asymptotic behaviours (3.14*a*,*b*) necessary to impose boundary conditions on the shear-layer, we plot $\mathscr{J}_c$ versus ε_o in figure 9.

The nature of the solutions portrayed in figures 8 and 9 may be understood, by considering the limiting cases of large and small ε_o. In the large-conductance limit

$$\varepsilon_o \gg 1, \tag{4.8}$$

solutions are approximated by the $\varepsilon_o \uparrow \infty$ solution of § 3. The graph of $\Omega_o = \omega_o$ versus A plotted solid in figure 3 for $\zeta_i = 4/5$ deserves comparison with the $\varepsilon_o \downarrow 0$ curve in figure 8(*b*) for $\zeta_i = 1/2$. Both graphs exhibit reverse flow $\Omega_o < 0$ for sufficiently small A near the poles. For the Hollerbach *et al.* (2007) boundary radii (4.2), formulae (A 1*c*) and (A 5) with (4.3*a*) determine, in turn,

$$\varpi_m \equiv A_m/A_c \approx 0.5108 \qquad \text{and} \qquad \mathscr{J}_c \approx 0.3459. \tag{4.9a,b}$$

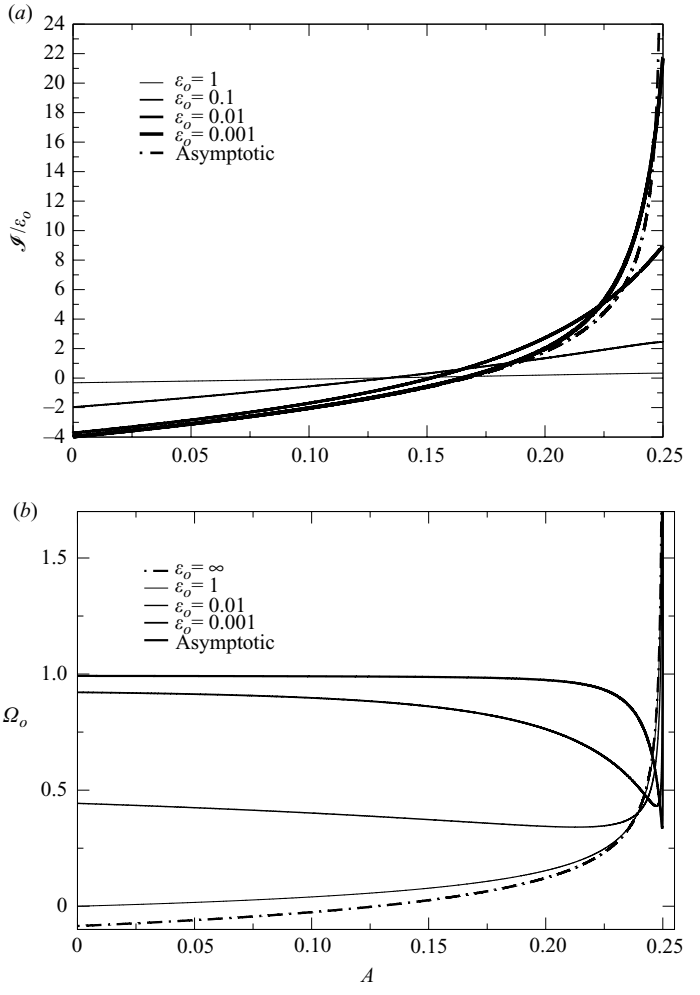

FIGURE 8. Case (4.2), $r_i = 1$, $r_o = 2$ ($\zeta_i = 1/2$); $\sigma_i^S \uparrow \infty$: the numerical solution of the mainstream equations (4.7*a*,*b*), for various values of ε_o. (*a*) The scaled mainstream electric current $\mathscr{J}(A)/\varepsilon_o$ is plotted versus A (solid lines). The $\mathscr{P}$-outer solution (4.11*b*) is used for the asymptotic $\varepsilon_o \downarrow 0$ solution shown by the dot-dashed line; it is hardly distinguishable from the numerical solution for $\varepsilon_o = 0.001$. (*b*) The outer boundary mainstream angular velocity Ω_o (see (4.6*b*)) is plotted versus A using solid lines, as in (*a*). The perfectly conducting boundary solution of Appendix A is used for the asymptotic $\varepsilon_o \uparrow \infty$ solution shown by the dot-dashed lines.

They fix the large-ε_o asymptote for $\mathscr{J}_c$ in figure 9.

In the low-conductance limit

$$\varepsilon_o \ll 1, \tag{4.10}$$

(4.7*a*,*b*) provide a singular perturbation problem for which separate asymptotic solutions apply in two overlapping domains spanning the mainstream polar region $\mathscr{P}$. We refer to the smaller domain close to the $\mathscr{C}$-line as the '$\mathscr{P}$-inner' region and the larger domain continuing as far as the polar axis as the '$\mathscr{P}$-outer' region.

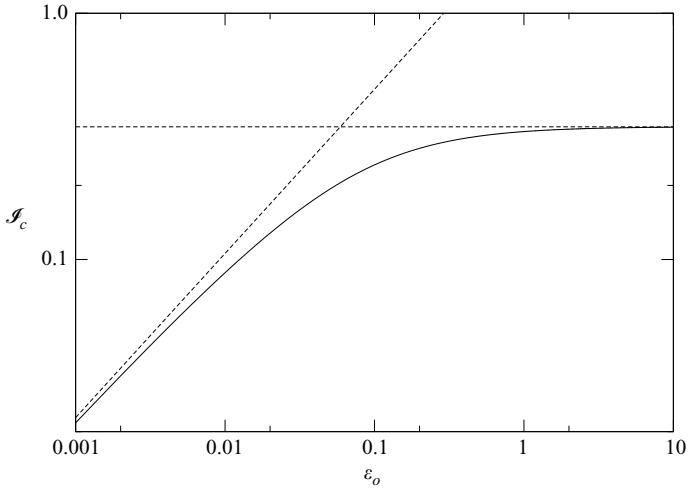

FIGURE 9. Case (4.2), $\zeta_i = 1/2$; $\sigma_i^S \uparrow \infty$: log–log plot of $\mathscr{J}_c \equiv \mathscr{J}(A_c)$ as a function of ε_o determined by the numerical solution of (4.7*a*,*b*). The asymptotes $\mathscr{J}_c/\varepsilon_o^{2/3} \approx 2.2948$ for $\varepsilon_o \downarrow 0$, determined by (4.15*a*,*b*) and (4.3*a*), and $\mathscr{J}_c \approx 0.3459$ for $\varepsilon_o \uparrow \infty$ (see (4.9*b*)) are indicated by the dashed lines.

The $\mathscr{P}$-outer solution $\mathscr{G}$ of (4.7) is small throughout its domain and is given almost everywhere by

$$\mathscr{G} \approx -\varepsilon_o A/\Phi_o' = \varepsilon_o 4 r_o^3 A \Phi_o = \varepsilon_o (A/A_c)\sqrt{1-(A/A_c)}, \tag{4.11a}$$

$$\mathscr{J} \equiv -\mathscr{G}' \approx -\frac{\mathscr{G}}{A} + \varepsilon_o r_o \frac{A/A_c}{\sqrt{1-(A/A_c)}}, \tag{4.11b}$$

which is illustrated by the dot-dashed curve in figure 8(*a*). Since solution (4.11*a*,*b*) shows that $\mathscr{G}$ and $\mathscr{J}$ are $O(\varepsilon_o)$ it follows from (4.6*b*) and in turn from (2.19*b*) that

$$\Omega_o \approx 1 \qquad \text{and} \qquad \mathscr{F} \approx 1 \tag{4.11c,d}$$

respectively. It means that fluid throughout the $\mathscr{P}$-outer region is locked to the inner sphere as it is for the case of Dormy *et al.* (2002) of an insulating outer boundary. The difference between solution (2.36) of Dormy *et al.* (2002), which yields $\mathscr{G} \to 0$ in our limit $M \uparrow \infty$ (see (4.4)), for zero ε_o and solution (4.11*a*) of the present work for small but finite ε_o arises because the electric current at the outside is returned by the Hartmann layer in the former $\varepsilon_o = 0$ case but by the solid in the latter $0 < \varepsilon_o \ll 1$ case.

The singular asymptotic behaviour of (4.11*a*,*b*), as $A \uparrow A_c$, may be conveniently expressed in terms of $\Phi_o = \sqrt{1-(A/A_c)}/(2r_o^2)$ (see (2.13*b*)):

$$\mathscr{G} \approx 2\varepsilon_o r_o^2 \Phi_o, \qquad \mathscr{J} \approx \frac{\varepsilon_o}{2 r_o \Phi_o} \qquad \text{as} \qquad \Phi_o \downarrow 0. \tag{4.12a,b}$$

The divergence of $\mathscr{J}$ and the corresponding electric potential ϑ (see (4.5)) as the $\mathscr{C}$-line is approached, indicated by (4.12*b*), means that the solution cannot meet the $\mathscr{C}$-line boundary conditions at $A = A_c$, where $\Phi_o = 0$. Here the $\mathscr{P}$-outer solution fails and must be matched instead with the $\mathscr{P}$-inner solution needed to remove this singular behaviour.

The leading-order asymptotic form of the differential equation (4.7*a*) for the $\mathscr{P}$-inner problem is

$$r_o^{-2}\beta_i \mathscr{J}' - \varepsilon_o^{-1} 2 r_o \Phi_o' \mathscr{G} = 1 \qquad \text{with} \qquad \mathscr{G}' = -\mathscr{J}, \tag{4.13a,b}$$

where $\beta_i \equiv r_o^2 \Phi_Q$ (see (B 2*c*)). At the outer edge of the $\mathscr{P}$-inner region the solution of (4.13) must match (4.12*a*,*b*), as well as meet the boundary condition $\mathscr{G}_c \equiv \mathscr{G}(A_c) = 0$ on the $\mathscr{C}$-line. The analytic solution (C 5) to this problem given in Appendix C shows that the A-flux scale $\Delta_{\mathscr{P}}$ of the $\mathscr{P}$-inner region is $O(\varepsilon_o^{2/3})$. From it we may introduce the length $\delta_{\mathscr{P}}$ defined by the coordinate $(s, z) \approx (r_o, \delta_{\mathscr{P}})$, where the magnetic field line $A = A_c - \Delta_{\mathscr{P}}$ intersects the outer sphere (cf. definition (3.19) of $\delta_{\mathscr{C}}$). In fact, we choose

$$\delta_{\mathscr{P}}/r_o = (\Delta_{\mathscr{P}}/A_c)^{1/2} \equiv (\varepsilon_o \beta_i)^{1/3}. \tag{4.14}$$

The main finding of Appendix C is that

$$\mathscr{J}_c = \varepsilon_o^{2/3} \beta_i^{-1/3} r_o J_c, \tag{4.15a}$$

where, from (C 5) and (C 6),

$$J_c = (2\pi/\sqrt{3})\,\mathrm{Ai}(0) \approx 1.2879. \tag{4.15b}$$

This result provides the small-ε_o asymptote for $\mathscr{J}_c$ in figure 9.

Throughout most of the $\mathscr{P}$-inner region, Ω_o is given correct to leading order by $\Omega_o = -\Phi_o' \varepsilon_o^{-1} \mathscr{G}/A$ (see (C 9)) because the other contribution $-\Phi_o' \mathscr{J}$ to expression (4.6*b*) is negligible, as is made self-evident by examination of (C 7). As the $\mathscr{C}$-line is approached, however, the small $A_c - A$ approximation $\mathscr{G} \approx \mathscr{J}_c(A_c - A)$, $\mathscr{J} \approx \mathscr{J}_c$ of the solution of (4.13) becomes valid so that whereas $\mathscr{G}$ tends to zero, $\mathscr{J}$ remains finite. In consequence the term $-\Phi_o' \mathscr{J}$ neglected in (4.6*b*) must be reinstated leading to the form

$$\Omega_o \approx \frac{\mathscr{J}_c}{2r_o}\left[\varepsilon_o^{-1}\left(\frac{A_c - A}{A_c}\right)^{1/2} + \left(\frac{A_c}{A_c - A}\right)^{1/2}\right] \qquad \text{for} \qquad A \uparrow A_c \tag{4.16}$$

given by (C 8). It possesses the minimum

$$\Omega_{o\,min} = \varepsilon_o^{-1/2} r_o^{-1} \mathscr{J}_c \qquad \text{at} \qquad A_c - A = \varepsilon_o A_c \ll (\varepsilon_o \beta_i)^{2/3} A_c = \Delta_{\mathscr{P}} \tag{4.17a}$$

well inside the $\mathscr{P}$-inner region sufficiently close to the $\mathscr{C}$-line for formula (4.16) to be valid. Moreover, use of our asymptotic result (4.15*a*) shows that

$$\Omega_{o\,min} = \varepsilon_o^{1/6} \beta_i^{-1/3} J_c. \tag{4.17b}$$

So the monotonic decrease of Ω_o predicted by (C 9) from unity in the $\mathscr{P}$-outer region to almost zero in the $\mathscr{P}$-inner region is terminated at $A = (1 - \varepsilon_o)A_c$ after which Ω_o diverges. The way that this minimum develops as ε_o decreases is illustrated in figure 8(*b*).

4.2. *Large but finite Hartmann number*

In the previous section, § 4.1, we formally took the limit $M \uparrow \infty$ so that we could ignore the electric current carried by the outer Hartmann layer ($1 - \mathscr{L}_o = 0$; see (2.33*a*)). Moreover, in the small-ε_o limit, the mainstream 'relative' tangential electric field component determined by Ohm's law, $(E_\theta + s\Omega B_r)_o = \mathscr{J} B_{\theta o}$, at the edge of the outer Hartmann layer (see the discussion above (3.2)) was negligible in Ohm's law throughout both the $\mathscr{P}$-outer (as evinced by solution (4.11*a*)) and $\mathscr{P}$-inner (manifest by the absence of the term $-\Phi_o' \mathscr{J}$ in the asymptotic form (4.13*a*) of (4.7*a*)) regions.

In this section we consider the double limit

$$M \gg 1, \qquad \varepsilon_o \ll 1\,; \tag{4.18}$$

we no longer neglect the jump $B_o^S + \mathscr{G}/s_o$ in the tangential magnetic field across the Hartmann layer but continue to neglect the contribution $\mathscr{J} B_{\theta o}$ to Ohm's law. Under these assumptions, the angular velocity jump (2.32) across the outer Hartmann layer becomes

$$\omega_o \approx \frac{\varepsilon_o^{-1}\mathscr{G}/A}{2r_o^3\left(2\Phi_o + (\varepsilon_o M)^{-1}\right)}, \tag{4.19}$$

in which the term $(\varepsilon_o M)^{-1}$ has been reinstated in the denominator and the term $\mathscr{J}$ has been neglected in the numerator. Likewise, the fraction of the electric current leaving the mainstream and captured by the Hartmann layer given by (2.33*b*) reduces to

$$1 - \mathscr{L}_o = 1\,/\left(\varepsilon_o M_o^{loc} + 1\right) \tag{4.20}$$

(see (2.27)), which is $O(1)$ when $\varepsilon_o M_o^{loc} = O(1)$ but tends to zero as $M \uparrow \infty$.

In the $\mathscr{P}$-outer region, we make the approximation $\mathscr{G} \ll 1$ just as before in § 4.1, which implies by (2.21*d*) and (4.6*a*) that $\Omega_i \approx \Omega_o\,(=\omega_o)$ and $(1 - \Omega_i =)\,\omega_i \approx 0$ respectively. In consequence the fluid remains locked to the inner sphere with all the angular velocity jump occurring across the outer Hartmann layer. With $\Omega \approx \omega_o \approx 1$, the solution determined by (2.19*b*) and (4.19) is

$$\mathscr{F} \approx 1, \qquad \mathscr{G} \approx (A/A_c)\left(\varepsilon_o\sqrt{1-(A/A_c)} + \tfrac{1}{2}\mathscr{M}^{-1}\right) \tag{4.21a,b}$$

(c.f. Mizerski & Bajer 2007, p. 265, equation (7.8*a*,*b*)), where $2\mathscr{M} = M/r_o^2$ (see (2.5)). We emphasize that expression (4.21*b*) for $\mathscr{G}$ differs from our earlier result (4.11*a*) by the presence of the extra term $\mathscr{M}^{-1}(A/2A_c)$.

Since our only alteration to the analysis of § 4.1 is to replace expression (4.6*b*) for ω_o by (4.19), the corresponding modified form of the governing equations (4.13*a*,*b*) for the $\mathscr{P}$-inner problem is simply

$$-r_o^{-2}\beta_i\,\mathscr{G}'' + \left(\varepsilon_o\sqrt{1-(A/A_c)} + \tfrac{1}{2}\mathscr{M}^{-1}\right)^{-1}\mathscr{G} = 1. \tag{4.22}$$

Scale analysis of (4.22) shows that the A-flux scale $\Delta_{\mathscr{P}}$ given previously by (4.14) now satisfies

$$\beta_i^{-1}(\Delta_{\mathscr{P}}/A_c)^2 \sim \varepsilon_o(\Delta_{\mathscr{P}}/A_c)^{1/2} + \tfrac{1}{2}\mathscr{M}^{-1} \tag{4.23}$$

so that $\Delta_{\mathscr{P}}/A_c = (\varepsilon_o\beta_i)^{1/3}$ when $(\varepsilon_o\beta_i)^{-1} \ll (2\mathscr{M}/\beta_i)^{3/4}$, as given before by (4.14), while $\Delta_{\mathscr{P}}/A_c \sim (\beta_i/2\mathscr{M})^{1/2}$ when $(2\mathscr{M}/\beta_i)^{3/4} \ll (\varepsilon_o\beta_i)^{-1}$.

Crucial to our understanding of the asymptotic solutions is the relative size of the flux widths $\Delta_{\mathscr{P}}$ of the $\mathscr{P}$-inner mainstream region determined by the above estimates and $\Delta_{\mathscr{C}}$ of the shear-layer on $\mathscr{C}$ given by (3.18*b*):

$$\frac{\Delta_{\mathscr{P}}}{\Delta_{\mathscr{C}}} = \begin{cases} (\varepsilon_o\beta_i)^{2/3}(\mathscr{M}/\alpha_i)^{1/2} & \text{for} \quad 1 \ll (\varepsilon_o\beta_i)^{-1} \ll (2\mathscr{M}/\beta_i)^{3/4}, \\ (\beta_i/2\alpha_i)^{1/2} & \text{for} \quad (2\mathscr{M}/\beta_i)^{3/4} \ll (\varepsilon_o\beta_i)^{-1}. \end{cases} \tag{4.24}$$

Here the ratio $\alpha_i/\beta_i = 2(2-\zeta_i)\zeta_i^2$ (see (B 2*c*,*d*)) is of order unity, except when the radius ratio $\zeta_i \equiv r_i/r_o$ is small. In reality the $\mathscr{P}$-inner region only exists when $\Delta_{\mathscr{P}} \gg \Delta_{\mathscr{C}}$, which occurs when $\varepsilon_o M^{3/4} \gg 1$. In that case, the analysis of § 4.1 is valid, and the shear-layer solution is fixed by the value of $\mathscr{J}_c$. Otherwise, when either $\varepsilon_o M^{3/4} \ll 1$

or $\varepsilon_o M^{3/4} = O(1)$, we must ignore the $\mathscr{P}$-inner solution and match the shear-layer solution directly with $\mathscr{P}$-outer solution (4.21) (see also the discussion following (5.8)).

4.3. *The shear-layer on $\mathscr{C}$ for $\Delta_{\mathscr{P}} = O(\Delta_{\mathscr{C}})$*

The nature of the shear-layer on $\mathscr{C}$ depends critically on Hartmann jump conditions at the outer boundary. For that the local Hartman number at $A = A_{\mathscr{C}} \equiv A_c - \Delta_{\mathscr{C}}$ determined by (2.27) and (3.19) is

$$M^{loc}_{o\mathscr{C}} \equiv M^{loc}_o(A_{\mathscr{C}}) = 2\alpha_i^{1/4}\mathscr{M}^{3/4}. \tag{4.25}$$

The corresponding electric current leakage parameter (4.20) evaluated at $A = A_{\mathscr{C}}$, namely $\mathscr{L}_{o\mathscr{C}} \equiv \mathscr{L}_o(A_{\mathscr{C}})$, is given by

$$1 - \mathscr{L}_{o\mathscr{C}} = 1 \big/ \big(\varepsilon_o M^{loc}_{o\mathscr{C}} + 1\big)\,. \tag{4.26}$$

When $\Delta_{\mathscr{P}} = O(\Delta_{\mathscr{C}})$ or equivalently in view of (4.24)

$$\big(\tfrac{1}{2}\varepsilon_o M^{loc}_{o\mathscr{C}} =\big)\ \alpha_i^{1/4}\varepsilon_o\mathscr{M}^{3/4} = O(1), \tag{4.27}$$

the shear-layer equation (3.20) continue to apply, but as the results of this section show, the boundary conditions (3.21) and (3.22), that their solutions must satisfy, are modified.

Central to the boundary condition modification is the matching of the shear-layer solution at large n with the $\mathscr{P}$-outer mainstream solution (4.21*a*,*b*) for small $A_c - A (> 0)$. When expressed in terms of the shear-layer coordinates l, n, its asymptotic form is

$$\mathscr{F} \approx 1, \qquad \mathscr{G} \approx \varepsilon_o(\Delta_{\mathscr{C}}/A_c)^{1/2} n^{1/2} + \tfrac{1}{2}\mathscr{M}^{-1}. \tag{4.28a,b}$$

From them we may construct expressions for the shear-layer-dependent variables $V_\pm$ defined by (3.16). Then in place of (3.21) we obtain

$$M^{1/2}V_\pm \to \begin{cases} s_c \mp r_o^2 s_c^{-1}\big(1 + \varepsilon_o M^{loc}_{o\mathscr{C}}\, n^{1/2}\big) & \text{as} \quad n \uparrow \infty, \\ s_c & \text{as} \quad n \downarrow -\infty \end{cases} \tag{4.29}$$

on $0 < l < 1$.

The vanishing of the angular velocity jump on the inner sphere $\omega_i \approx 0$, implying $\Omega_i \approx 1$, determines the condition

$$M^{1/2}(V_+ + V_-) = 2s_Q \tag{4.30}$$

at $l = 0$, while at the equator E_o on the outer sphere, condition (4.19), in which $\mathscr{G}$ is replaced by $-sB$, together with the symmetry condition (2.9) determines

$$V_+ = \begin{cases} -V_-/\big(1 + 2(\varepsilon_o M^{loc}_{o\mathscr{C}})^{-1} n^{-1/2}\big) & \text{for} \quad n > 0, \\ V_- & \text{for} \quad n < 0 \end{cases} \tag{4.31}$$

at $l = 1$. It should, however be noted that the boundary condition for $n > 0$ at $l = 1$ relies on the the thin shell approximation. For it to be valid, the θ-length scale $\delta_{\mathscr{C}}$ (see (3.19)) tangent to the outer boundary of the shear-layer must be large compared with the outer solid boundary thickness δ_o:

$$\delta_o/r_o \ll \delta_{\mathscr{C}}/r_o = (\alpha_i/\mathscr{M})^{1/4} = O(\varepsilon_o^{1/3}), \tag{4.32}$$

in the parameter range (4.27) for which this estimate applies.

In the low-conductance limit $M^{loc}_{o\mathscr{C}}/2 = \alpha_i^{1/4}\mathscr{M}^{3/4} \ll \varepsilon_o^{-1}$ ($\mathscr{L}_{o\mathscr{C}} \approx 0$), the boundary conditions (4.29)–(4.31) reduce to those employed by Dormy *et al.* (2002, equations (3.10)–(3.12)) and their shear-layer results apply. Interestingly, on reinstating the small

$O(\varepsilon_o \mathscr{M}^{3/4})$ correction terms in the boundary conditions (4.29) and (4.31), Mizerski & Bajer (2007) found, albeit in a plane layer geometry, a corresponding small $O(\varepsilon_o \mathscr{M}^{3/4})$ increase in the super-rotation rate above the lowest order asymptotic value of Dormy *et al.* (2002).

In the alternative limit $1 \ll \varepsilon_o^{-1} \ll \alpha_i^{1/4} \mathscr{M}^{3/4} = M_{o\mathscr{C}}^{loc}/2$ ($\mathscr{L}_{o\mathscr{C}} \approx 1$), the boundary conditions (4.30) and (4.31) at $l=0$ and $l=1$ reduce to (3.22) appropriate to a perfectly conducting outer boundary. Likewise the matching condition (4.29) reduces to $V_\pm \to 0$ as $n \downarrow -\infty$ on $0 \leqslant l \leqslant 1$, in agreement with (3.21). However, as $n \uparrow \infty$, (4.29) gives

$$MB \approx \pm M^{1/2} V_\pm \to -\varepsilon_o M_{o\mathscr{C}}^{loc} r_o^2 s_c^{-1} n^{1/2} \tag{4.33}$$

on $0 \leqslant l \leqslant 1$, which does not correspond to that given by (3.21). The reason for this discrepancy is that we have effectively extended the shear-layer outwards to include the $\mathscr{P}$-inner mainstream. Accordingly the matching condition, (4.33) corresponds to matching directly with the $\mathscr{P}$-outer mainstream solution $\mathscr{G} \approx 2\varepsilon_o r_o^2 \Phi_o$ (see (4.12*a*)). This is an unnecessary complication that we obviously ignore.

In summary, we have identified three parameter ranges in which shear-layer solutions have different scales:

$$V_\pm = \begin{cases} O(1) & \text{for} \quad \varepsilon_o^{-1} \ll 1 \ll M^{3/4}, \\ O(\varepsilon_o^{2/3}) & \text{for} \quad 1 \ll \varepsilon_o^{-1} \ll M^{3/4}, \\ O(M^{-1/2}) & \text{for} \quad 1 \ll M^{3/4} \ll \varepsilon_o^{-1}. \end{cases} \tag{4.34}$$

Throughout the first two ranges ($\mathscr{L}_{o\mathscr{C}} \approx 0$) the value of $V_\pm$ is determined by the perfectly conducting boundary calculation of § 3.3 via the value of $\mathscr{J}_c$. In the first range, $\varepsilon_o^{-1} \ll 1 \ll M^{3/4}$, $\mathscr{J}_c$ is given by (A 5) of Appendix A; in the second range, $1 \ll \varepsilon_o^{-1} \ll M^{3/4}$, $\mathscr{J}_c$ is given by by (4.15) of § 4.1; while in the intermediate range, $\varepsilon_o = O(1)$ ($0 < \mathscr{L}_{o\mathscr{C}} < 1$), the numerical solution of (4.7) determines the values of $\mathscr{J}_c$ plotted versus ε_o in figure 9. The solution for $V_\pm$ in the third range $1 \ll M^{3/4} \ll \varepsilon_o^{-1}$ ($\mathscr{L}_{o\mathscr{C}} \approx 1$) is determined simply by the insulating boundary results of Dormy *et al.* (2002) while Mizerski & Bajer (2007) essentially investigated the the influence of small but finite $\varepsilon_o M^{3/4}$ in their plane geometry.

The shear-layer results for the first two combined ranges $\varepsilon_o^{-1} \ll M^{3/4}$ and the third range $M^{3/4} \ll \varepsilon_o^{-1}$ have clearly distinguishable character. The transition, when $\varepsilon_o = O(M^{-3/4})$, between the two cases is more complicated. For that, the shear-layer problem of § 3.3 must be solved subject to the boundary conditions (4.29)–(4.31) just derived. Then the problem for each distinct value of $\varepsilon_o M^{3/4}$ needs to be solved separately. Since the accurate solution of the shear-layer equations for any one particular case, as in § 3.3 for $\varepsilon_o \uparrow \infty$, is a very considerable undertaking, we have not attempted the time-consuming numerical calculations needed to solve the shear-layer equations for a variety of distinct values of $\varepsilon_o M^{3/4}$. We remark, however, that solutions for $M^{3/4} \ll \varepsilon_o^{-1}$ (the Dormy *et al.* (2002) problem) are recovered in the limit $\varepsilon_o \downarrow 0$.

5. Shear-layer super-rotation

The objective of this section is to determine the magnitude of the super-rotation in the shear-layer and to make comparisons with the results of Mizerski & Bajer (2007) and Hollerbach *et al.* (2007). The case of an inner perfectly conducting boundary is considered in § 5.1, for which we simply apply the results of § 4. Since both Mizerski & Bajer (2007) and Hollerbach *et al.* (2007) considered the case of an inner boundary of the same conductivity as the fluid, we address this issue in § 5.2. Recall, however,

that the results of § 3.2 showed that this distinction has little effect on the solution (see figure 5), and so we ignore the distinction when making comparisons with Mizerski & Bajer (2007) in section § 5.1.

5.1. *Inner perfectly conducting boundary $\varepsilon_i^{-1}=0$: a comparison with Mizerski & Bajer (2007)*

Our shear-layer estimates (4.34) show that the corresponding peak values of Ω, which occur in them, are

$$\Omega_{max} = \begin{cases} O(M^{1/2}) & \text{for} \quad \varepsilon_o^{-1} \ll 1 \ll M^{3/4}, \\ O(\varepsilon_o^{2/3} M^{1/2}) & \text{for} \quad 1 \ll \varepsilon_o^{-1} \ll M^{3/4}, \\ O(1) & \text{for} \quad 1 \ll M^{3/4} \ll \varepsilon_o^{-1}. \end{cases} \tag{5.1}$$

As explained in § 4.2, throughout the first two ranges

$$\varepsilon_o^{-1} \ll M^{3/4}, \tag{5.2}$$

the amplitude of $V_{\pm}$ is proportional to $\mathscr{J}_c$ (see the shear-layer boundary condition (3.21)). As a consequence, the peak value Ω_{max} of the angular velocity is determined as a linear function of $\mathscr{J}_c$ by the formula

$$\Omega_{max} = \Upsilon \mathscr{J}_c, \qquad \text{in which} \qquad \Upsilon \equiv \left[\Omega_{max} / \mathscr{J}_c\right]_{\varepsilon_o \uparrow \infty} \tag{5.3a,b}$$

is given by the solution of the shear-layer problem outlined in § 3.3 for the perfectly conducting boundary case $\varepsilon_o \uparrow \infty$. The numerical results of § 3.4, for the $\zeta_i = 0.8$ case, give $[\Omega_{max}]_{\varepsilon_o \uparrow \infty} \approx 0.0823 \times M^{1/2}$. So, since the mainstream analytic solution of Appendix A determines $[\mathscr{J}_c]_{\varepsilon_o \uparrow \infty} \approx 1.766$ (see (3.15*b*)), we deduce that

$$\Upsilon \approx 0.0466 \times M^{1/2} \qquad \text{for} \qquad \zeta_i = 0.8. \tag{5.4}$$

In general, the value of $\mathscr{J}_c$ needed in (5.3*a*) is obtained from the numerical solution of the mainstream equations (4.7*a*,*b*). Results for the $\zeta_i = 0.5$ case are illustrated in figure 9, which provides a plot of $\mathscr{J}_c$ versus ε_o. Though the analytic solution gives $[\mathscr{J}_c]_{\varepsilon_o \uparrow \infty} \approx 0.35$ (see (4.9*a*)), we did not solve the corresponding shear-layer problem to determine $[\Omega_{max}]_{\varepsilon_o \uparrow \infty}$, and so we are unable to evaluate formula (5.3*b*) for Υ. Nevertheless, since $\Omega_{max} \propto \mathscr{J}_c$, figure 9 may also be regarded as a plot of a scaled Ω_{max} versus ε_o. Interestingly the plot bears a striking resemblance to the plot of Mizerski & Bajer (2007) for U_{max} (cf. our Ω_{max}) versus σ_o^S/σ in figure 6(*b*) of their work, where for their boundary of finite thickness σ_o^S/σ is similar to our ε_o. Whereas the results of Mizerski & Bajer (2007) are obtained from the numerical integration of the full system of governing differential equations, albeit in their planar geometry, our figure 9 results are derived from an asymptotic theory valid for $\varepsilon_o^{-1} \ll M^{3/4}$.

Though the value of Ω_{max} in the last range $M^{3/4} \ll \varepsilon_o^{-1}$ of (5.1) is determined directly by the insulating outer boundary $\varepsilon_o \downarrow 0$ theory of Dormy *et al.* (2002), it too is dependent on the radius ratio ζ_i. Dormy *et al.* (2002) obtained

$$\Omega_{max} \approx 1.4147 \qquad \text{for} \qquad \zeta_i = 0.35, \qquad \varepsilon_o = 0. \tag{5.5}$$

Unfortunately, since all asymptotic results obtained in this paper pertain to other ζ_i-values, namely $\zeta_i = 0.8$ and 0.5, we are unable to provide a unified quantification of Ω_{max} over the entire range $0 \leqslant \varepsilon_i < \infty$ for any single value of ζ_i. This deficiency is due to the enormously time-consuming numerical computations needed to solve the shear-layer problem, which prohibits our presentation of other results.

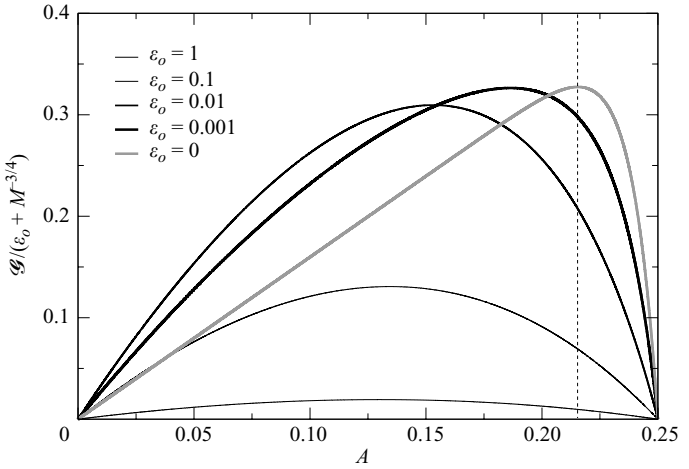

FIGURE 10. Case (4.2), $\zeta_i = 1/2$; $\varepsilon_i = 1$: the scaled mainstream electric current flux $\mathscr{G}(A)/(\varepsilon_o + M^{-3/4})$ plotted versus A, which solves (2.35), when $M = 10^4$, for various values of ε_o. The value of A, at which the limiting case $\varepsilon_o = 0$ has its maximum, is identified by the vertical dotted line; it is shown to indicate the $\mathscr{C}$-line shear-layer flux width $O(M^{-1/2})$ in the vicinity of $A = A_c = 0.25$, where matching with the shear-layer ought to occur.

5.2. *Inner finitely conducting boundary $\varepsilon_i = O(1)$: a comparison with Hollerbach et al. (2007)*

Hollerbach *et al.* (2007) considered the case of a thin outer solid boundary (like us) and a solid inner sphere with the same conductivity as the fluid $\sigma_i^S = \sigma$ (unlike us). Of course, our thin boundary theory does not apply to the thick inner boundary case of Hollerbach *et al.* (2007), but we believe that the results inside the fluid are not particularly sensitive to the precise form of the inner magnetic boundary condition. We attempt to make quantitative comparisons with Hollerbach *et al.* (2007) by solving the mainstream equation (2.35) subject to the boundary conditions $\mathscr{G}(0) = \mathscr{G}(A_c) = 0$ (valid for $\varepsilon_o^{-1} \ll M^{3/4}$) for the the $r_i = 1$, $r_o = 2$ case (see (4.2)) of Hollerbach *et al.* (2007) with $\varepsilon_i \equiv (\sigma_i^S/\sigma^S)(\delta_i/r_i)$ unity on the basis that $\delta_i = r_i$:

$$\zeta_i = 0.5, \qquad \varepsilon_i = 1. \tag{5.6a,b}$$

The dependence of the mainstream equation (2.35) on the finite conductance ε_i is captured by the angular velocity jump (2.32),

$$\omega_i = \frac{-\mathscr{J} + \varepsilon_i^{-1}\mathscr{G}/A}{2r_i^3\left(2\Phi_i + (\varepsilon_i M)^{-1}\right)}, \qquad \text{giving} \qquad \omega_i \approx \Phi_i'(\mathscr{J} - \varepsilon_i^{-1}\mathscr{G}/A) \tag{5.7a,b}$$

when $\varepsilon_i = O(1)$ and $M \gg 1$, across the inner boundary Hartmann layer. So any feature for our $\varepsilon_i = 1$ case, that differs from the $\varepsilon_i^{-1} = 0$ case, stems from the extra term $-\Phi_i'\mathscr{G}/A$ (5.7*b*), absent in (3.2).

To identify any different character of the solution when $\varepsilon_i = 1$, we solved (2.35) as it stands, based on the full expression (5.7*a*) for ω_i rather than the approximated form (5.7*b*). Results for the $M = 10^4$ case are used to obtain the plots of $\mathscr{G}/(\varepsilon_o + M^{-3/4})$ versus ε_o portrayed in figure 10; the cosmetic scale factor $1/(\varepsilon_o + M^{-3/4})$ is included to reduce the changes in the magnitude of $\mathscr{G}$, which occur as ε_o is increased from 0 to 1 in figure 10 across $\varepsilon_o = O(M^{-3/4}) \sim 10^{-3}$. Note that the locations of the

maxima $A = A_{max}$ of $\mathscr{G}$ in figure 10 compare reasonably with the zeros of $-\mathscr{J} = \mathscr{G}'$ in figure 8(a). As the value of ε_o decreases the comparison becomes less favourable because the term $(\varepsilon_o M)^{-1}$ in (4.19) was omitted in the derivation of the solutions portrayed in figure 8(a). The corresponding failure of the compatibility of the graphs in figures 8(a) and 10 is most pronounced close to A_c. It reflects how we deal with the Hartmann layer jump condition at the outer boundary rather than the differing jump conditions at the inner boundary. With that proviso, the evidence of figures 8(a) and 10 suggests that the qualitative features of the mainstream solution for $\varepsilon_i = 1$ with ω_i given by (5.7a) are adequately described by the solution for $\varepsilon_i^{-1} = 0$ with ω_i given by (4.6a).

To interpret the results in figures 8(a) and 10, it is helpful first to examine the plot of $\mathscr{J}_c$ versus ε_o in figure 9. It shows that the small and large asymptotic behaviours (for the case $\varepsilon_o^{-1} = 0$ at any rate) are reached below ~ 0.01 and above ~ 1 respectively. It means that behaviour of the small- and large-ε_o type should be interpreted in the sense of $10\varepsilon_o \ll 1$ and $10\varepsilon_o \gg 1$ respectively. The fact that $10\varepsilon_o$ is the relevant number rather than ε_o simply reflects the fact that we have neglected the factors dependent on the the radii r_i and r_o in our order of magnitude estimates. With this proviso, the $\varepsilon_o = 1$, 0.1 and 0.01 cases illustrated in figure 10 appear to typify $\varepsilon_o^{-1} \ll 1$, $\varepsilon_o^{-1} = O(1)$ and $1 \ll \varepsilon_o^{-1} \ll M^{3/4}$ behaviour respectively and are largely independent of the large value of M. The $\varepsilon_o = 0.001 = M^{-3/4}$ and $\varepsilon_o = 0$ cases illustrated in figure 10 possibly reflect the $\varepsilon_o^{-1} = O(M^{3/4})$ and $M^{3/4} \ll \varepsilon_o^{-1}$ regimes respectively.

The $\varepsilon_o = 0$ solution plotted in figure 10 has clear outer and inner structures. The $\mathscr{P}$-outer solution is

$$\mathscr{G} \approx \tfrac{1}{2}\mathscr{M}^{-1}(A/A_c) \tag{5.8}$$

(see (2.36) and also (4.21b)). The $\mathscr{P}$-inner governing equation is $-r_o^{-2}\beta_i\,\mathscr{G}'' + 2\mathscr{M}\mathscr{G} = 1$ (cf. (4.13a,b)). Its solution describes the boundary layer of flux width $O(M^{-1/2})$ visible in the right part of figure 10 in the vicinity of $A = A_c$. This is the same size as the flux width $\Delta_{\mathscr{C}}$ of shear-layer on $\mathscr{C}$. As explained at the end of § 4.2, the $\mathscr{P}$-inner region does not exist, and the Dormy *et al.* (2002) type of shear-layer appropriate to an insulating outer boundary must be matched directly to the $\mathscr{P}$-outer solution (5.8). Therefore, we have marked the maximum of $\mathscr{G}$ for the $\varepsilon_o = 0$ solution by the vertical line in figure 10 because it roughly indicates the location $A = A_{\mathscr{C}} \equiv A_c - \Delta_{\mathscr{C}}$ of the outer edge of the shear-layer, for all values of ε_o. All solutions portrayed to the right of that line are unphysical and should be ignored.

The remaining question about the other cases $\varepsilon_o \neq 0$ concerns the type of shear-layer onto which the mainstream solutions portrayed in figure 10 ought to match. To that end, we consider the values $\mathscr{G}_{\mathscr{C}}$ and $-\mathscr{J}_{\mathscr{C}}$, of $\mathscr{G}$ and its slope $\mathscr{G}'$ on the vertical line $A = A_{\mathscr{C}}$ of figure 10. If $\mathscr{J}_{\mathscr{C}}$ is reasonably well approximated by the value $\mathscr{J}_c$ at $A = A_c$, as in the $\varepsilon_o = 1$, 0.1 cases, matching to the § 3.3 type of shear-layer ($\varepsilon_o^{-1} = 0$) with $\mathscr{J}_{\mathscr{C}} = \mathscr{J}_c$ ought to be appropriate. If on the other hand, $\mathscr{J}_{\mathscr{C}}/\mathscr{J}_c \ll 1$, matching the Dormy *et al.* (2002) type of shear-layer ($\varepsilon_o = 0$) to $\mathscr{G} = \mathscr{G}_{\mathscr{C}}$ appears to be sensible. The remaining two cases $\varepsilon_o = 0.01$, 0.001 are intermediate in the sense that $\mathscr{J}_{\mathscr{C}}/\mathscr{J}_c = O(1)$. Therefore we propose that they should be matched to a § 4.3 ($\Delta_{\mathscr{P}} = O(\Delta_{\mathscr{C}})$) type of shear-layer intermediate between the other two extreme cases.

We now consider the numerical results of Hollerbach *et al.* (2007), for case (5.6), illustrated in the left panel of figure 2 of their work, in which $\log(\Omega_m)$ is plotted versus $\log(Ha^2)$ in the range $10^{3/2} \leqslant Ha \leqslant 10^3$ for various values of ε_o. These data are reproduced by the dashed curves in figure 11 of the current paper, which plots

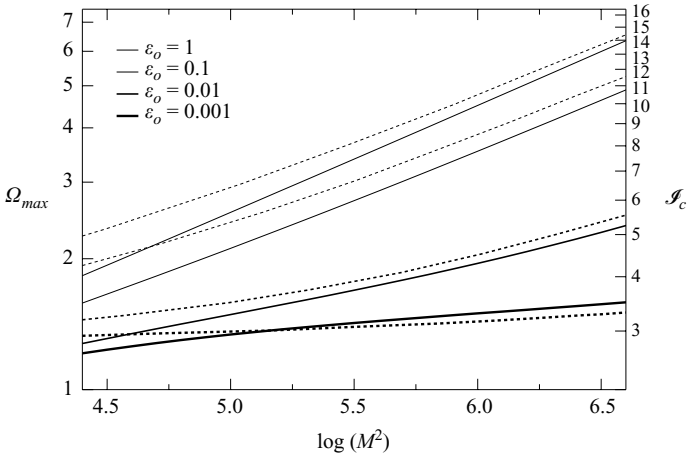

FIGURE 11. Case (4.2), $\zeta_i = 1/2$; $\varepsilon_i = 1$: the values of $\mathscr{J}_c \equiv \mathscr{J}(A_c)$ (right scale), determined by the solutions of (2.35) for various ε_o, plotted versus $\log(M^2)$ by the continuous lines. For comparison, the maximum value of the angular velocity Ω_{max} (left scale), determined by the data of figure 2 of Hollerbach *et al.* (2007), is illustrated by the dashed lines.

$\Omega_{max} = \Omega_m$ versus $\log(M^2)$, where $(\mathscr{M} \equiv) M/(2r_o^2) = Ha$. In the same figure we plot (continuous lines) the values of $\mathscr{J}_c$ obtained by solving the mainstream equation (2.35) subject to the boundary conditions $\mathscr{G}(0) = \mathscr{G}(A_c) = 0$ in exactly the same way that the results illustrated in figure 10 were obtained.

The comparison in figure 11 is motivated by result (5.3*a*), which indicates that $\Omega_{max} = \Upsilon \mathscr{J}_c$ when $\varepsilon_o^{-1} \ll M^{3/4}$. As noted in § 5.1, our numerical solution in § 3.4 of the shear-layer equations was for the radius ratio $\zeta_i = 4/5$, and so value (5.4) of the constant of proportionality Υ, which it determines, does not apply in the $\zeta_i = 1/2$ case of Hollerbach *et al.* (2007). Nevertheless, the logarithm of (5.3*a*) gives $\log(\Omega_{max}) = \log(\mathscr{J}_c) + \log \Upsilon$, where $\log \Upsilon =$ constant. Since both Ω_{max} and $\mathscr{J}_c$ are plotted using a log-scale in figure 11, the only indeterminacy is the location of the origin $\mathscr{J}_c = 1$ (i.e. $\log(\mathscr{J}_c) = 0$) on the $\mathscr{J}_c$-axis. Without that information, we estimate its location so as to obtain a reasonable comparison with the results of Hollerbach *et al.* (2007) in the domain $\varepsilon_o^{-1} \ll M^{3/4}$ (see (5.2)), where we expect our asymptotic results to apply, i.e. for large M and moderate ε_o at the top right-hand corner of the figure.

We recall that figure 10 was plotted for the $\log(M^2) = 8$ case, which lies beyond the right-hand end of the scale in figure 11. Since our asymptotic theory is based on $M \gg 1$, we chose the large value $M = 10^4$ to emphasize the distinct character of the solution for the various values of ε_o considered. Guided by our interpretation of the results in figure 10, we expect that our asymptotic results will agree with the numerical results of Hollerbach *et al.* (2007) on increasing M for the $\varepsilon_o = 1$, 0.1 cases, though some reasonable agreement might be achieved for the $\varepsilon_o = 0.01$ case, with perhaps vague agreement for the $\varepsilon_o = 0.001$ case. We do not reproduce the data of Hollerbach *et al.* (2007) for the $\varepsilon_o = 0$ case, as formula (5.3*a*) is certainly inapplicable. The comparisons of the trends with increasing M in figure 11 are remarkably encouraging despite the fact that the inner sphere boundary conditions of Hollerbach *et al.* (2007) are not properly modelled by our asymptotic theory and that our use of the formula $\Omega_{max} = \Upsilon \mathscr{J}_c$ only applies when $\varepsilon_o^{-1} \ll M^{3/4}$.

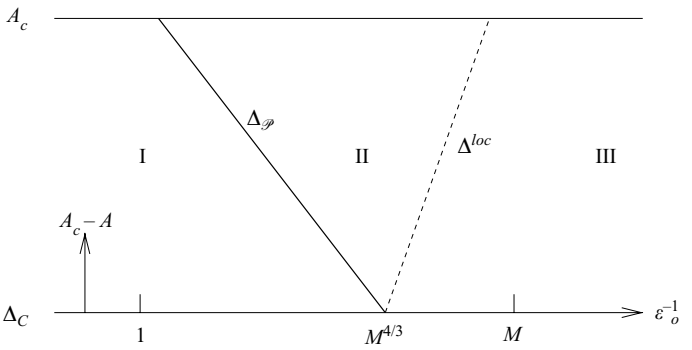

FIGURE 12. A log–log plot of $A_c - A$ versus ε_o^{-1}, in which we identify regions of the polar-$\mathscr{P}$ mainstream, between the pole (the upper horizontal line $A_c - A = 0$) and the edge of the shear-layer (the lower horizontal line $A_c - A = \Delta_{\mathscr{C}}$). The oblique thick solid line $A_c - A = \Delta_{\mathscr{P}}$ and thick dashed line $A_c - A = \Delta^{loc}$ divide the space from left to right into three regions, namely I, II and III. Ferraro's law holds in II and III but not in I. Electric current leakage into the outer boundary is blocked in III but is substantial in I and II.

6. Concluding remarks

The analysis in this paper has extended the mainstream and free shear-layer theory of Dormy *et al.* (2002) for the case of a conducting inner boundary and an insulating outer boundary to more general boundary conductivities. The key simplification that has permitted progress for other boundary conductivities is the thin shell boundary approximation (2.31*a*), which ensures that all magnetic boundary conditions are local. Then the structure of the mainstream solution is governed by the second-order ordinary differential equation (2.35), which we have solved for various values $\varepsilon_{(i,o)}$ of the relative conductances (2.31*c*) of the inner, i, and outer, o, boundaries.

Most of our large-M study has been concerned with the nature of the flow for the case of a perfectly conducting inner boundary over the complete range of conductance ε_o of the outer boundary. The mainstream solution of § 4.1 for $\varepsilon_o = O(1)$ is important because it describes the transition between the limiting cases of large and small ε_o. When $\varepsilon_o \gg 1$, the complete solution including both the mainstream and shear-layer solutions are approximated well by the case of the perfectly conducting outer boundary, $\varepsilon_o \uparrow \infty$, in which the electric field vanishes. An essential feature of the polar-$\mathscr{P}$ mainstream flow is its failure to meet Ferraro's law of isorotation, as evinced before in the cylindrical shell model of Bühler (2009). When $\varepsilon_o = O(1)$, the electric field in the outer solid can no longer be neglected (see (4.6*b*) and the discussion that follows it), which leads to a modification of the mainstream solution. On decreasing ε_o, Ferraro's law of isorotation continues to fail in a $\mathscr{P}$-inner region $0 < A_c - A \leqslant O(\Delta_{\mathscr{P}}) = O(\varepsilon_o^{2/3} A_c)$ (see (4.14)) neighbouring the $\mathscr{C}$-line shear-layer identified by domain I in figure 12. The size of the $\mathscr{P}$-inner region continues to shrink until the magnetic flux width $\Delta_{\mathscr{P}}$ coincides with the shear-layer width $A_c - A_{\mathscr{C}} = \Delta_{\mathscr{C}} = O(M^{-1/2} A_c)$ (see (3.18*b*)) at $\varepsilon_o^{-1} = O(M^{3/4})$, where the $\mathscr{P}$-inner region disappears. Note also that $A = A_{\mathscr{C}}$ identifies the $A_c - A = \Delta_{\mathscr{C}}$ axis of figure 12.

In parameter regimes, for which the induced azimuthal magnetic field B_ϕ^* in the polar mainstream region is sufficiently small so that Ferraro's law of isorotation is met (domains II and III in figure 12), the value of B_ϕ^* is related simply, via the local outer boundary Hartmann number $M_o^{loc}(A)$ (see (2.27)), to its value $B_\phi^*|_{\varepsilon_o \downarrow 0}$ (see (2.36))

in the insulating limit $\varepsilon_o \downarrow 0$ by

$$\frac{B^*_\phi}{B^*_\phi|_{\varepsilon_o\downarrow 0}} = \begin{cases} \varepsilon_o M^{loc}_o(A) & \text{for} \quad 1 \ll \varepsilon_o^{-1} \ll M^{3/4}, \\ \varepsilon_o M^{loc}_o(A) + 1 & \text{for} \quad M^{3/4} \ll \varepsilon_o^{-1} \ll M, \\ 1 & \text{for} \quad M \ll \varepsilon_o^{-1}. \end{cases} \tag{6.1a,b,c}$$

The first case (6.1*a*), which provides the dimensional form of solution (4.11*a*), only applies in the $\mathscr{P}$-outer region, $A_c - A \gg \Delta_{\mathscr{P}}$, exterior to the $\mathscr{P}$-inner region discussed in the previous paragraph. The second and third cases (6.1*b*,*c*), determined by (4.21*b*) and (2.36) respectively, apply throughout the polar region, $A_c - A \gg \Delta_{\mathscr{C}}$. The third case (6.1*c*) identifies the parameter range for which the insulting outer boundary solution of Dormy *et al.* (2002) pertains.

A more illuminating form of the intermediate case (6.1*b*), which encompasses the limiting cases (6.1*a*,*c*) is

$$(1 - \mathscr{L}_o)\, B^*_\phi = B^*_\phi\big|_{\varepsilon_o\downarrow 0}, \tag{6.2}$$

where $1 - \mathscr{L}_o = 1/(\varepsilon_o M^{loc}_o(A) + 1)$ (see (4.20)) is the fraction of the electric current inflow from the mainstream retained by the Hartmann layer; $\mathscr{L}_o$ is the remaining fraction leaked into the solid boundary. In essence, the electric current flow in the mainstream must increase with ε_o to maintain the state of the Hartmann layer. Since M^{loc}_o (see (2.27)) decreases from the value M/r_o^2 at the pole to zero at the equator, where it meets the shear-layer, the importance of the electric current leakage decreases with latitude in concert.

The outer Hartmann layer and solid boundary currents become comparable, when $\mathscr{L}_o = 1/2$, at the location $A = A^{loc}$, where

$$\varepsilon_o M^{loc}_o(A^{loc}) = 1 \qquad \text{implying} \qquad \Delta^{loc} \equiv A_c - A^{loc} = \left(\frac{r_o^2}{\varepsilon_o M}\right)^2 A_c \tag{6.3}$$

(see (2.27)). So on decreasing ε_o^{-1} across the intermediate range (6.1*b*), the value of Δ^{loc} decreases from A_c at the pole, when $\varepsilon_o^{-1} = M/r_o^2$, to $\Delta_{\mathscr{C}}$ at the edge of the shear-layer, when $\varepsilon_o^{-1} = O(M^{3/4})$. Essentially electric current leakage into the outer boundary is blocked, $\mathscr{L}_o = 0$, in the region $0 < A_c - A \leqslant O(\Delta^{loc}) = O((\varepsilon_o M)^{-2} A_c)$ neighbouring the $\mathscr{C}$-line shear-layer identified by domain III in figure 12, while leakage is substantial, $\mathscr{L}_o \approx 1$, in domains I and II.

The nature of the shear-layer on the $\mathscr{C}$-line, $A = A_c$, is dependent on the magnitude

$$\mathscr{L}_{o\mathscr{C}} = \mathscr{L}_o(A_{\mathscr{C}}) = \varepsilon_o M^{loc}_{o\mathscr{C}} \big/ \left(\varepsilon_o M^{loc}_{o\mathscr{C}} + 1\right) \qquad \left(M^{loc}_{o\mathscr{C}} \equiv M^{loc}_o(A_{\mathscr{C}})\right) \tag{6.4}$$

(see (4.25) and (4.26)) of the electric current leakage into the outer boundary near the equator at $A = A_{\mathscr{C}}$, determined by the shear-layer flux width $\Delta_{\mathscr{C}}$. There are two limiting cases of small and large electric current leakage, which are respectively

$$\mathscr{L}_{o\mathscr{C}} = O(\varepsilon_o M^{3/4}) \qquad \text{for} \qquad \varepsilon_o M^{3/4} \ll 1, \tag{6.5a}$$

$$1 - \mathscr{L}_{o\mathscr{C}} = O(\varepsilon_o^{-1} M^{-3/4}) \qquad \text{for} \qquad 1 \ll \varepsilon_o M^{3/4}. \tag{6.5b}$$

Firstly, in the small-ε_o limit, $\varepsilon_o M^{3/4} \ll 1$, the insulating outer boundary shear-layer solution of Dormy *et al.* (2002) applies. Its distinctive character stems from the fact that the total electric current carried by the shear-layer is determined by the jump in value of $s^* B^*_\phi$ from zero in the equatorial $\mathscr{E}$-region to $-(r_o^*/L^*)^2\sqrt{\mu_0\rho\nu\eta}$ in the polar $\mathscr{P}$-region. The latter is the dimensional form of (2.36) at the $\mathscr{C}$-line, $A = A_c$, obtained with the help of the Hartmann number definition (1.1*a*). Significantly, this

condition is independent of both ε_o and the typical size B_0^* of the applied meridional magnetic field $\boldsymbol{B}_M^*$, as the polar-$\mathscr{P}$ mainstream is entered. Mizerski & Bajer (2007) considered the influence of $O(\varepsilon_o M^{3/4})$ corrections and found a small increase in the super-rotation rate of $O(\varepsilon_o M^{3/4}\Omega_i^{S*})$ above the $O(\Omega_i^{S*})$ value of Dormy *et al.* (2002). Their result may be explained by the terms proportional to $\varepsilon_o M_{o\mathscr{C}}^{loc}$ appearing in the shear-layer boundary conditions (4.29) and (4.31), as mentioned in the paragraph following (4.32).

Secondly, in the large-ε_o limit, $1 \ll \varepsilon_o M^{3/4}$, the perfectly conducting boundary shear-layer solution applies. The magnitude of Ω^* inside the shear-layer is fixed by the jump $\Theta_{\mathscr{C}}$ of the electric potential across it, which in turn is proportional to the polar mainstream electric current $\mathscr{J}_c \boldsymbol{B}_M^*/(\mu_0 L^*)$ at the $\mathscr{C}$-line (see (3.12*a*) and (3.24*d*)). In contrast to the small-ε_o shear-layer solution, which is constrained by the total electric current flow along it, the electric potential constraint across it is dependent on both ε_o (via $\mathscr{J}_c$; see figure 9) and $\boldsymbol{B}_M^*$. Our result, that the maximum super-rotation is $\Omega_{max}^* = O(M^{1/2}\Omega_i^{S*})$ in the limit $\varepsilon_o \uparrow \infty$ (see § 3.3), is consistent with the results of Bühler (2009) for his fluid bounded by perfectly conducting cylindrical shells. Moreover, our predictions over the entire large-ε_o range, $1 \ll \varepsilon_o M^{3/4}$, explain the substantial values of Ω_{max}^* found in the interesting numerical results of Hollerbach *et al.* (2007), as discussed in § 5.2.

We wish to thank the anonymous referees for very helpful comments. We also acknowledge the support of the CNRS/RS International Joint Project grant for travel support during the period 2006–2009. A.M.S. visited ENS, Paris (24–28 October 2006, 22–23 January 2007); E.D. visited MRI, University of Exeter (20–24 September 2006, 18–23 February 2008); and together we visited the School of Mathematics and Statistics, University of Newcastle-upon-Tyne (4–9 August 2008). We wish to thank all three institutions for their support.

Appendix A. The perfectly conducting boundary solution

The value of $\mathscr{G}$ obtained by integrating $(\Phi_i - \Phi_o)\mathscr{G}' = A_m - A$ given by (3.8) (see also (2.13*b*)) with $\mathscr{J} = -\mathscr{G}'$ may be expressed in the form

$$\mathscr{G}(A) = \varpi_m\, g_0(\varpi) - g_1(\varpi) \qquad \text{with} \qquad \varpi \equiv 2r_o A = A/A_c, \tag{A 1a,b}$$

where to meet the boundary condition conditions $\mathscr{G}(0) = 0$ and $\mathscr{G}(A_Q) = 0$ (see (3.10)) we choose $g_0(0) = g_1(0) = 0$ and

$$\varpi_m \equiv 2r_o A_m = A_m/A_c = g_1(1)/g_0(1) \tag{A 1c}$$

respectively. Our result is

$$g_0(\varpi) = \frac{1}{2}\int_0^{\varpi} \frac{1}{\zeta_i^{-2}\sqrt{1-\zeta_i\varpi} - \sqrt{1-\varpi}}\,\mathrm{d}\varpi, \tag{A 2a}$$

$$g_1(\varpi) = \frac{1}{2}\int_0^{\varpi} \frac{\varpi}{\zeta_i^{-2}\sqrt{1-\zeta_i\varpi} - \sqrt{1-\varpi}}\,\mathrm{d}\varpi, \tag{A 2b}$$

where $\zeta_i \equiv r_i/r_o$ (see (B 1*d*)). The values of these integrals are

$$g_0(\varpi) = \frac{\gamma_i^2}{1-\zeta_i}\left[\widehat{g}_0\left(\sqrt{1-\zeta_i\varpi}\,;\,\zeta_i\gamma_i\right) + \zeta_i^2\widehat{g}_0\left(\sqrt{1-\varpi}\,;\,\zeta_i^{-1}\gamma_i\right)\right], \tag{A 3a}$$

$$g_1(\varpi) = \frac{\gamma_i^2}{1-\zeta_i}\left[\zeta_i^{-1}\widehat{g}_1\left(\sqrt{1-\zeta_i\varpi}\,;\,\zeta_i\gamma_i\right) + \zeta_i^2\widehat{g}_1\left(\sqrt{1-\varpi}\,;\,\zeta_i^{-1}\gamma_i\right)\right], \tag{A 3b}$$

where

$$\gamma_i^2 \equiv \frac{\zeta_i(1-\zeta_i)}{1-\zeta_i^3} = \frac{\zeta_i}{1+\zeta_i+\zeta_i^2} \tag{A 3c}$$

and

$$\widehat{g}_0(\chi\,;\xi) = 1-\chi-\xi\,\tan^{-1}\left[\frac{\xi(1-\chi)}{\xi^2+\chi}\right], \qquad \frac{\mathrm{d}\widehat{g}_0}{\mathrm{d}\chi} = -\frac{\chi^2}{\xi^2+\chi^2}, \tag{A 4a,b}$$

$$\widehat{g}_1(\chi\,;\xi) = -\frac{1}{3}(1-\chi^3) + (1+\xi^2)\,\widehat{g}_0(\chi\,;\xi), \qquad \frac{\mathrm{d}\widehat{g}_1}{\mathrm{d}\chi} = -\frac{\chi^2(1-\chi^2)}{\xi^2+\chi^2}. \tag{A 4c,d}$$

Of particular interest is the value of (3.11), namely

$$\mathscr{J}_c \equiv -\mathscr{G}_c' = \frac{r_o\zeta_i^2(1-\varpi_m)}{\sqrt{1-\zeta_i}} = \frac{r_o(1-\varpi_m)}{2\beta_i}, \tag{A 5}$$

where $\beta_i = (1/2)\zeta_i^{-2}\sqrt{1-\zeta_i}$ (see (B 2c)).

Appendix B. The $\mathscr{C}$-line

Points on the $\mathscr{C}$-line $A = A_c \equiv 1/2r_o$ may be defined parametrically by

$$s = s_c(l(\zeta)) \equiv r_o\zeta^{3/2}, \qquad z = z_c(l(\zeta)) \equiv r_o\zeta(1-\zeta)^{1/2} \tag{B 1a,b}$$

(see (2.2a) and (2.4a)), where

$$\zeta \equiv r/r_o \qquad \text{and} \qquad \zeta_i \equiv r_i/r_o. \tag{B 1c,d}$$

Though s_c and z_c are defined here as functions of ζ, we have introduced the intermediate dependence on $l(\zeta)$, as defined below by (B 3), because the function $s_c(l)$ is needed for our application in § 3.3.

The value Φ_c of Φ (see (2.1a) and (2.2b)) on the $\mathscr{C}$-line is conveniently measured by

$$\beta(\zeta) \equiv -r_o^2\int_{E_o}\boldsymbol{B}_M\cdot\mathrm{d}\boldsymbol{x} = r_o^2\Phi_c = \tfrac{1}{2}\zeta^{-2}\sqrt{1-\zeta} \tag{B 2a}$$

(see (2.4b)), where $E_o : (r_o, 0)$ is the equator of the outer sphere. Likewise, we define

$$\begin{aligned}\alpha(\zeta) &\equiv -2\int_{E_o}s_c^2\boldsymbol{B}_M\cdot\mathrm{d}\boldsymbol{x} = 2\int_{E_o}s_c^2\mathrm{d}\Phi_c\\ &= 2\int_\zeta^1\frac{1-\frac{3}{4}\zeta}{(1-\zeta)^{1/2}}\,\mathrm{d}\zeta = (2-\zeta)\sqrt{1-\zeta}.\end{aligned} \tag{B 2b}$$

The values of β and α at the intersection of $\mathscr{C}$ with the inner sphere at $Q : (s_Q, z_Q)$ are

$$\beta_i \equiv \beta(\zeta_i) = r_o^2\Phi_Q = \tfrac{1}{2}\zeta_i^{-2}\sqrt{1-\zeta_i}, \tag{B 2c}$$

$$\alpha_i \equiv \alpha(\zeta_i) = (2-\zeta_i)\sqrt{1-\zeta_i}. \tag{B 2d}$$

For the shear-layer problem developed in § 3.3, the appropriate measure of distance along $\mathscr{C}$ from Q is distance weighted by $s_c^2|\boldsymbol{B}_M|$:

$$l(\zeta) \equiv \frac{2}{\alpha_i}\int_Q s_c^2 \boldsymbol{B}_M \cdot \mathrm{d}\boldsymbol{x} = 1 - \frac{\alpha(\zeta)}{\alpha_i}\,; \tag{B 3}$$

here l has been normalized by $2/\alpha_i$ so that $l(\zeta_i)=0$ at Q and $l(1)=1$ at E_o. Equation (3.20) governing the shear-layer $\mathscr{C}$ contains

$$\frac{1}{s_c}\frac{\mathrm{d}s_c}{\mathrm{d}l} = \frac{1}{s_c}\frac{\mathrm{d}s_c}{\mathrm{d}\zeta}\Big/\frac{\mathrm{d}l}{\mathrm{d}\zeta} = \frac{3\alpha_i}{4}\frac{\sqrt{1-\zeta}}{\zeta\left(1-\frac{3}{4}\zeta\right)}, \tag{B 4a}$$

while the differential equation (3.24*b*) for the shear-layer integral (3.24*a*) involves

$$\frac{\mathrm{d}\beta}{\mathrm{d}l} = -\frac{\alpha_i}{2}\left(\frac{r_o}{s_c}\right)^2. \tag{B 4b}$$

The parameter Ξ introduced in (3.12*b*) is

$$\Xi \equiv \frac{r_o^2}{2}\int_{\zeta_i}^1 \left(\frac{\beta_i}{\beta}-1\right)\zeta\,\mathrm{d}\zeta = \frac{r_o(r_o-r_i)}{140}\left(64\zeta_i^{-2}+32\zeta_i^{-1}-11-15\zeta_i\right). \tag{B 5}$$

Appendix C. The $\mathscr{P}$-inner mainstream solution

To solve the $\mathscr{P}$-inner equations (4.13*a*,*b*) we take advantage of the property $4r_o^3\Phi_o\Phi_o' = -1$ (see (2.14*b*)) and adopt Φ_o as the independent variable:

$$\frac{\beta_i}{r_o^3}\frac{\mathrm{d}\mathscr{J}}{\mathrm{d}\Phi_o} - \varepsilon_o^{-1}2\mathscr{G} = -4r_o^2\Phi_o, \qquad \frac{1}{r_o^2}\frac{\mathrm{d}\mathscr{G}}{\mathrm{d}\Phi_o} = 4r_o\Phi_o\mathscr{J}. \tag{C 1a,b}$$

On making the change of variables

$$\mathscr{J} = \frac{\varepsilon_o r_o^2}{\delta_{\mathscr{P}}}J, \qquad \mathscr{G} = \frac{\varepsilon_o\delta_{\mathscr{P}}}{r_o}G, \qquad \Phi_o = \frac{\delta_{\mathscr{P}}}{2r_o^3}\varphi, \tag{C 2a,b,c}$$

where $\delta_{\mathscr{P}}$ is defined by (4.14), the system of equations (C 1) reduces to

$$\frac{\mathrm{d}J}{\mathrm{d}\varphi} - G = -\varphi, \qquad \frac{\mathrm{d}G}{\mathrm{d}\varphi} = \varphi J. \tag{C 3a,b}$$

From (C 3*a*) we deduce that the boundary condition $G(0)=0$ implies $\mathrm{d}J/\mathrm{d}\varphi=0$ at $\varphi=0$ while matching with the $\mathscr{P}$-outer solution (4.12*a*, *b*) requires $G\approx\varphi$ and $J\approx\varphi^{-1}$ respectively as $\varphi\uparrow\infty$.

Further differentiation of (C 3*a*) leads to the inhomogeneous Airy equation

$$\frac{\mathrm{d}^2J}{\mathrm{d}\varphi^2} - \varphi J = -1. \tag{C 4}$$

The solution, satisfying the boundary conditions $\mathrm{d}J/\mathrm{d}\varphi(0)=0$ and $\varphi J\to 1$ as $\varphi\uparrow\infty$, is

$$J(\varphi) = \pi\left[\mathrm{Ai}'(0)\,\mathrm{Gi}(\varphi) - \mathrm{Gi}'(0)\,\mathrm{Ai}(\varphi)\right]/\,\mathrm{Ai}'(0) \tag{C 5}$$

(see Abramowitz & Stegun 1964, pp. 446–448). Together with (C 2*a*) and (4.14) we obtain

$$\mathscr{J}_c = \mathscr{J}(A_c) = \varepsilon_o^{2/3}\beta_i^{-1/3}r_oJ_c, \qquad \text{where} \qquad J_c \equiv J(0). \tag{C 6a,b}$$

The angular velocity Ω_o defined by (4.6*b*) is

$$\Omega_o = \varphi^{-1}\left(G + \tfrac{1}{2}\varepsilon_o^{1/3}\beta_i^{-2/3}J\right). \tag{C 7}$$

Since $\varphi^{-1}G \to 1$ and $\varphi J \to 1$ as $\varphi \uparrow \infty$, (C 7) shows that in the same limit, $\Omega_o \to 1$ as required by matching to the $\mathscr{P}$-outer solution (4.11*b*). Upon substitution of the asymptotic behaviours $J \approx J_c$ and $\Omega_o \sim (1/2)J_c\varphi$, valid for small φ, into (C 7), we obtain

$$\Omega_o \sim \tfrac{1}{2}J_c\left(\varphi + \varepsilon_o^{1/3}\beta_i^{-2/3}\varphi^{-1}\right). \tag{C 8}$$

The result emphasizes the fact that though the $O(\varepsilon_o^{1/3})$ term in (C 7) is negligible throughout most of the $\mathscr{P}$-inner region leaving

$$\Omega_o \approx \varphi^{-1}G, \tag{C 9}$$

the omitted term must be reinstated, as in (C 8), when $\varphi = O(\varepsilon_o^{1/6}\beta_i^{-1/3})$.

REFERENCES

Abramowitz, M. & Stegun, I. A. 1964 *Handbook of Mathematical Functions*. Dover.

Bühler, L. 2009 On the origin of super rotating layers in magnetohydrodynamic flows. *Theoret. Comput. Fluid Dyn.* doi:10.1007/s00162-009-0111-z, online 1 July 2009.

Dormy, E. 1997 Modélisation numérique de la dynamo terrestre. PhD thesis, I.P.G., Paris.

Dormy, E., Cardin, P. & Jault, D. 1998 MHD flow in a slightly differentially rotating spherical shell, with conducting inner core, in a dipolar magnetic field. *Earth Planet. Sci. Lett.* **160**, 15–30.

Dormy, E., Jault, D. & Soward, A. M. 2002 A super-rotating shear layer in magnetohydrodynamic spherical Couette flow. *J. Fluid Mech.* **452**, 263–291.

Ferraro, V. C. A. 1937 Non-uniform rotation of the sun and its magnetic field. *Mon. Not. R. Astron. Soc.* **97**, 458–472.

Garaud, P. & Guervilly, C. 2009 The rotation rate of the solar radiative zone. *Astrophys. J.* **695**, 799–808.

Hartmann, J. 1937 Theory of the laminar flow of an electrically conductive liquid in a homogeneous magnetic field. *K. Dan. Vidensk. Selsk. Mat. Fys. Medd.* **15** (6), 1–28.

Hartmann, J. & Lazarus, F. 1937 Experimental investigations on the flow of mercury in a homogeneous magnetic field. *K. Dan. Vidensk. Selsk. Mat. Fys. Medd.* **15** (7), 1–45.

Hollerbach, R. 2000 Magnetohydrodynamical flows in spherical shells. In *Physics of Rotating Fluids* (ed. C. Egbers & G. Pfister), Lecture Notes in Physics, vol. 549, pp. 295–316. Springer.

Hollerbach, R. 2001 Super- and counter-rotating jets and vortices in strongly magnetic spherical Couette flow. In *Dynamo and Dynamics, a Mathematical Challenge* (ed. P. Chossat, D. Armbruster & I. Oprea), NATO Science Series II, vol. 26, pp. 189–197. Kluwer.

Hollerbach, R., Canet, E. & Fournier, A. 2007 Spherical Couette flow in a dipolar magnetic field. *Eur. J. Mech* B **26** (6), 729–737.

Hollerbach, R. & Skinner, S. 2001 Instabilities of magnetically induced shear layers and jets. *Proc. R. Soc. Lond.* A **457**, 785–802.

Hunt, J. C. R. & Malcolm, D. G. 1968 Some electrically driven flows in magnetohydrodynamics. Part 2. Theory and experiment. *J. Fluid Mech.* **33** (4), 775–801.

Hunt, J. C. R. & Shercliff, J. A. 1971 Magnetohydrodynamics at high Hartmann number. *Annu. Rev. Fluid Mech.* **3**, 37–62.

Kelley, D. H., Triana, S. A., Zimmerman, D. A., Tilgner, A. & Lathrop, D. P. 2007 Inertial waves driven by differential rotation in a planetary geometry. *Geophys. Astrophys. Fluid Dyn.* **101**, 469–487.

Mizerski, K. A. & Bajer, K. 2007 On the effect of mantle conductivity on the super-rotating jets near the liquid core surface. *Phys. Earth Planet. Inter.* **160**, 245–268.

Müller, U. & Bühler, L. 2001 *Magnetofluiddynamics in Channels and Containers*. Springer.

Nataf, H.-C., Alboussière, T., Brito, D., Cardin, P., Gagnière, N., Jault, D., Mason, J.-P. & Schmitt, D. 2006 Experimental study of super-rotation in a magnetostrophic spherical Couette flow. *Geophys. Astrophys. Fluid Dyn.* **100**, 281–298.

Roberts, P. H. 1967*a* *An Introduction to Magnetohydrodynamics*. Longmans.

Roberts, P. H. 1967*b* Singularities of Hartmann layers. *Proc. R. Soc. Lond.* A **300**, 94–107.

Shercliff, J. A. 1953 Steady motion of conducting fluids in pipes under transverse magnetic fields. *Proc. Camb. Phil. Soc.* **49**, 136–144.

Shercliff, J. A. 1956 The flow of conducting fluids in circular pipes under transverse magnetic fields. *J. Fluid Mech.* **1** (6), 644–666.

Soward, A. M. & Dormy, E. 2007 Boundary and shear layers in rotating (MHD) flows. In *Mathematical Aspects of Natural Dynamos* (ed. E. Dormy & A. M. Soward), The Fluid Mechanics of Astrophysics and Geophysics (series ed. A. M. Soward & M. Ghil), vol. 13, pp. 121–151. Grenoble Sciences and CRC Press.

Starchenko, S. V. 1998*a* Magnetohydrodynamic flow between insulating shells rotating in strong potential field. *Phys. Fluids* **10**, 2412–2420.

Starchenko, S. V. 1998*b* Strong potential field influence on slightly differentially rotating spherical shells. *Stud. Geoph. Geod.* **42**, 314–319.

Stewartson, K. 1966 On almost rigid rotation. Part 2. *J. Fluid Mech.* **26**, 131–144.

Walker, J. S. 1981 Magnetohydrodynamic flows in rectangular ducts with thin conducting walls. *J. Méc.* **20**(1), 79–112.

Zatmann, S. 2001 Phase relations for high frequency core mantle coupling and the Earth's axial angular momentum budget. *Phys. Earth Planet. Inter.* **121**, 163–178.